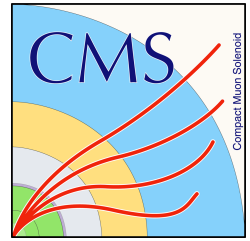

FPD Experimental Seminar – SLAC

7^{th} July 2020

Probing QCD using top quark pairs: latest results from CMS

Matteo M. Defranchis

content of the presentation

context

- the Standard Model and the top quark
  $\rightarrow$ focus on top quark mass
- the LHC and the CMS experiment

recent CMS results

- measurement of the $\mathrm{t\bar{t}}$ cross section at $\sqrt{s} = 13\,\mathrm{TeV}$
- extraction of m_t and α_S
- **first measurement of the running of the top quark mass**
- measurement of a triple-differential $\mathrm{t\bar{t}}$ cross section at $\sqrt{s} = 13\,\mathrm{TeV}$
- global QCD analysis with HERA DIS data: PDFs, α_S, m_t

quantum field theory based on principle
of **local gauge invariance**

$$\underbrace{SU(3)_c}_{\text{strong}} \otimes \underbrace{SU(2)_L \otimes U(1)_Y}_{\text{electroweak}}$$

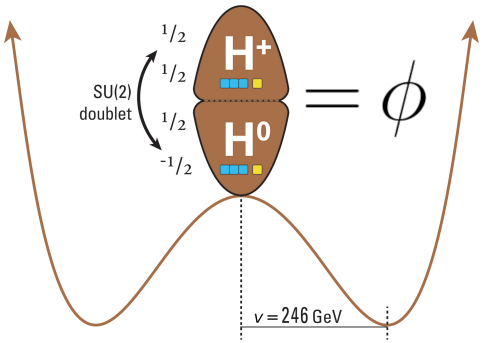

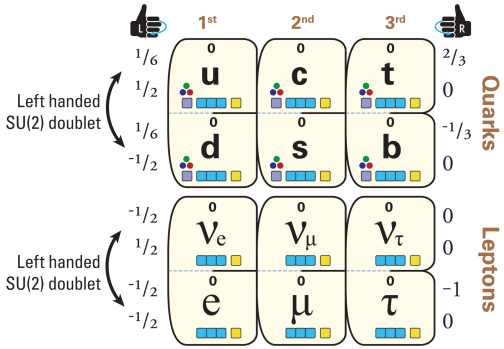

matter fields

gauge fields
(interactions)

$$V(\phi) = -\mu^2|\phi|^2 + \lambda|\phi|^4$$

mass term quartic coupling

quantum field theory based on principle of **local gauge invariance**

$$\underbrace{SU(3)_c}_{\text{strong}} \otimes \underbrace{SU(2)_L \otimes U(1)_Y}_{\text{electroweak}}$$

physical fields obtained after

- electroweak mixing
- spontaneous symmetry breaking

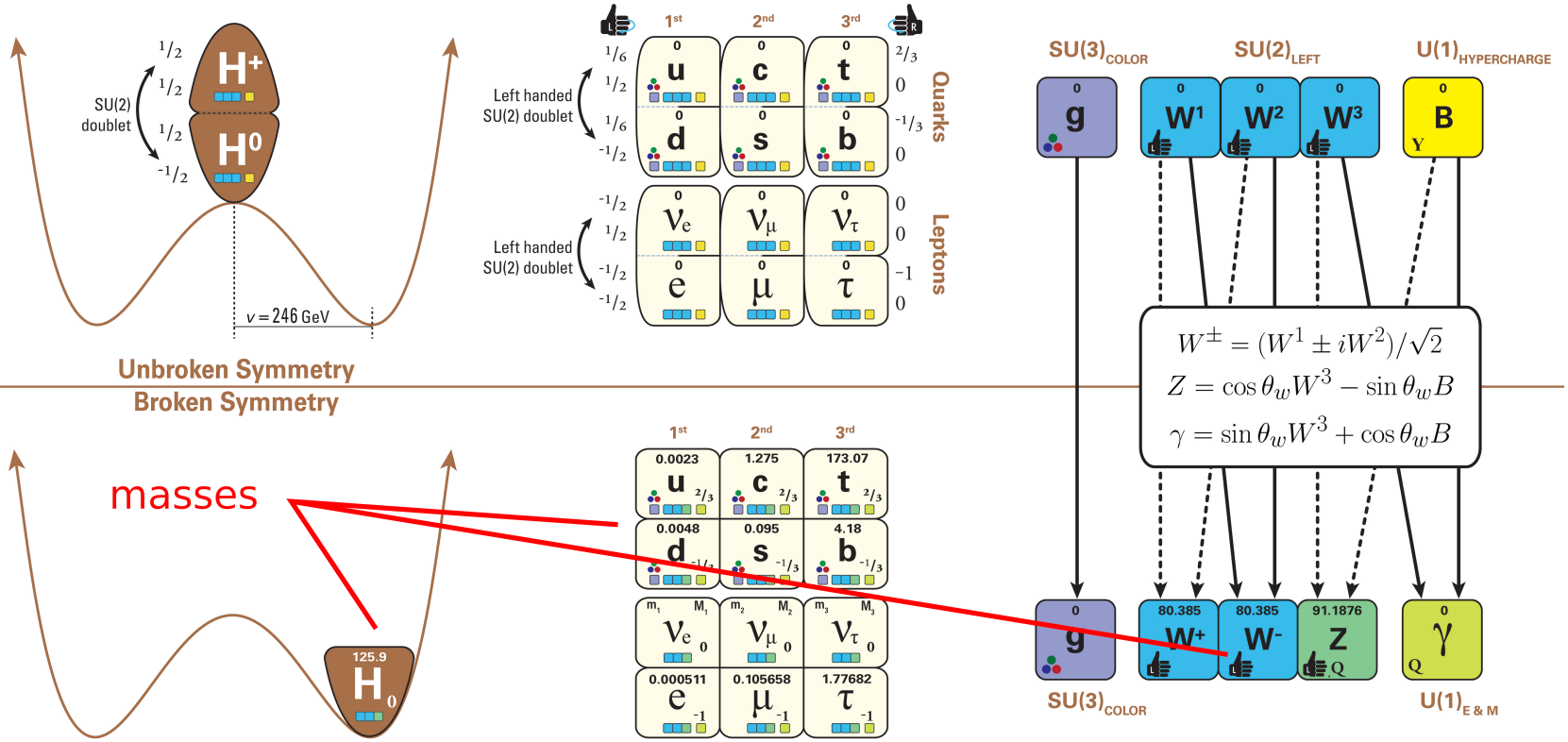

the Standard Model of particle physics

quantum field theory based on principle of **local gauge invariance**

$$\underbrace{SU(3)_c}_{\text{strong}} \otimes \underbrace{SU(2)_L \otimes U(1)_Y}_{\text{electroweak}}$$

physical fields obtained after

- electroweak mixing
- spontaneous symmetry breaking

$m_t \simeq 173\,\text{GeV} \rightarrow$ most massive SM particle

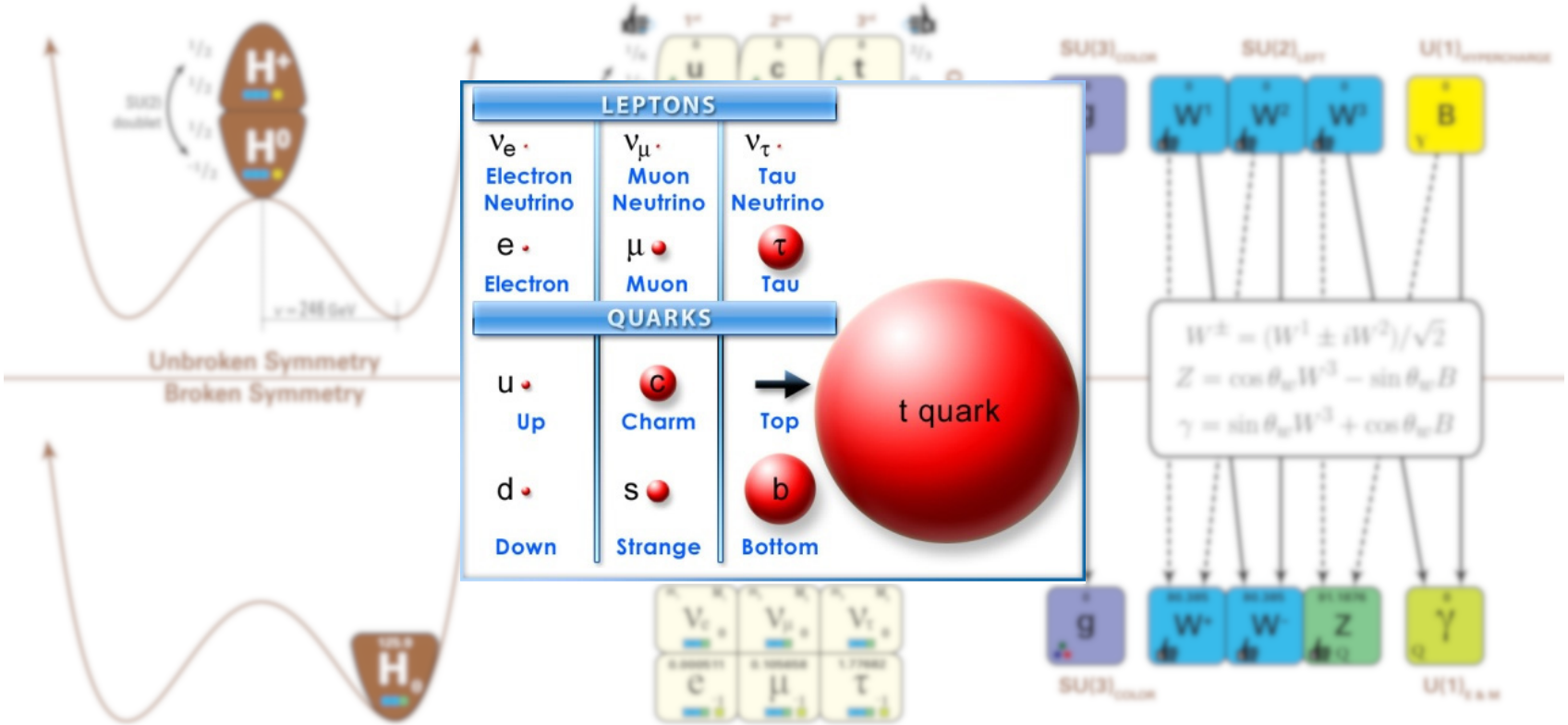

Quantum Chromodynamics

strong interaction of quarks and gluons
$\rightarrow$ 8 gluon fields

fundamental parameters

1. strong coupling constant α_S
2. quark masses

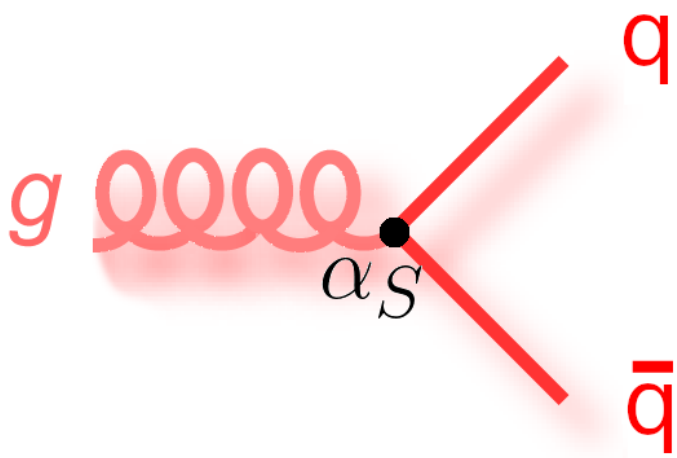

Quantum Chromodynamics

strong interaction of quarks and gluons
$\rightarrow$ 8 gluon fields

fundamental parameters

1. strong coupling constant α_S
2. quark masses

quantum corrections contain divergent loop diagrams $\Rightarrow$ **renormalization**

- infinities subtracted at scale μ_R and absorbed into bare parameters

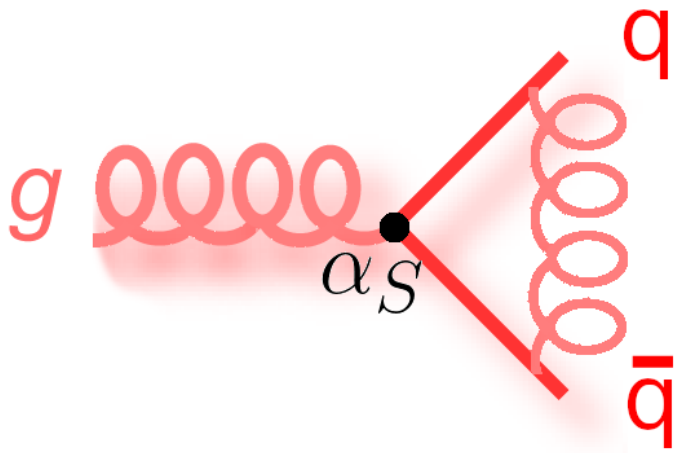

Quantum Chromodynamics

strong interaction of quarks and gluons
$\rightarrow$ 8 gluon fields

fundamental parameters

1. strong coupling constant α_S
2. quark masses

quantum corrections contain divergent loop diagrams $\Rightarrow$ **renormalization**

- infinities subtracted at scale μ_R and absorbed into bare parameters

running of $\alpha_S(Q)$

1. short distance $\rightarrow$ perturbative QCD
2. long distance $\rightarrow$ confinement
   $Q \sim \Lambda_{QCD} \simeq 250\,\text{MeV}$

$\rightarrow$ renormalization group equation (RGE) can be solved perturbatively

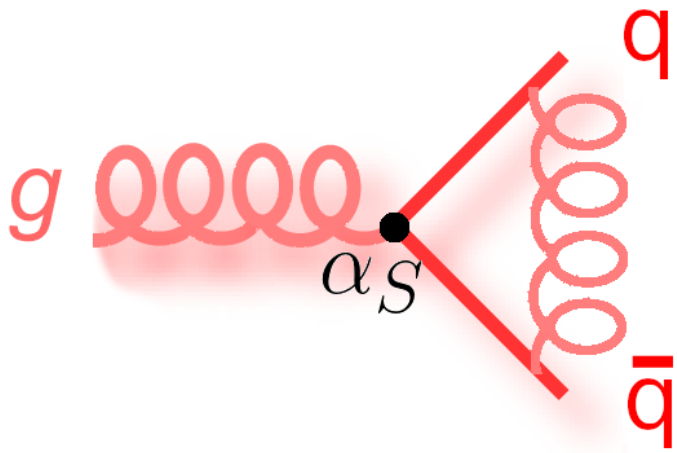

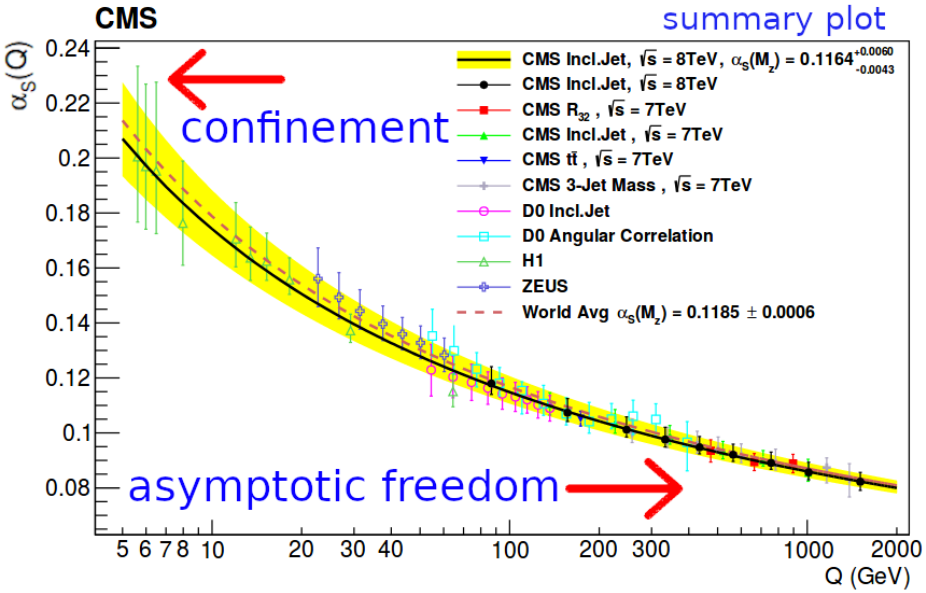

factorization of QCD

- long- and short-distance dynamics can be factorized at the scale μ_F

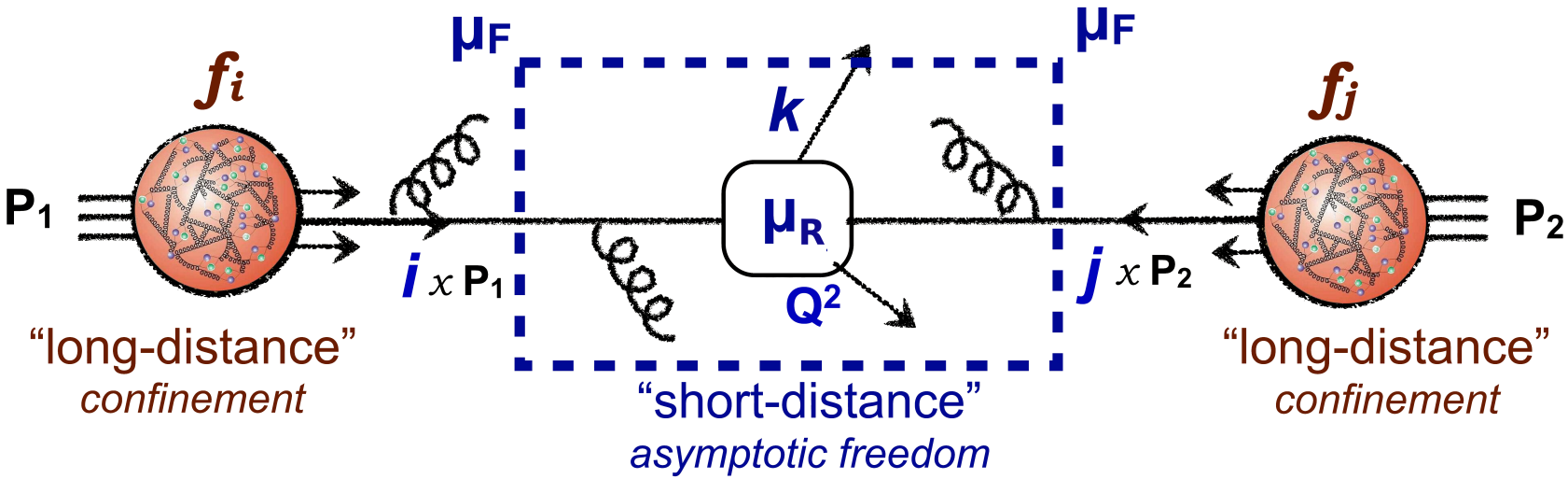

factorization of QCD

- long- and short-distance dynamics can be factorized at the scale μ_F
- convolution between proton (hadron) structure and partonic scattering

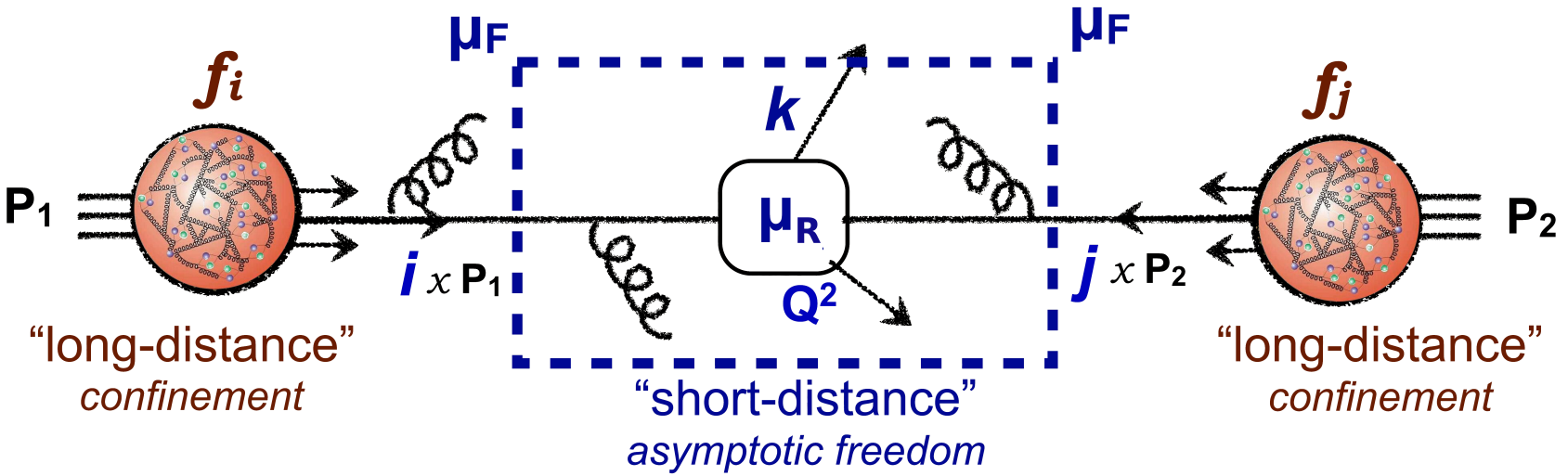

$$\sigma_{pp\to X} = \sum_{ij} f_i(x_1,\mu_F^2) \times f_j(x_2,\mu_F^2) \otimes \hat{\sigma}_{ij\to X}(x_1,x_2,\alpha_S(\mu_R),\frac{Q^2}{\mu_R},\frac{Q^2}{\mu_F})$$

prediction — proton structure — partonic cross section (pQCD)

→ variations of μ_R and μ_F estimate size of missing higher-order terms

quark masses in QCD

renormalization of m_q

- definition of m_q depends on renormalization procedure

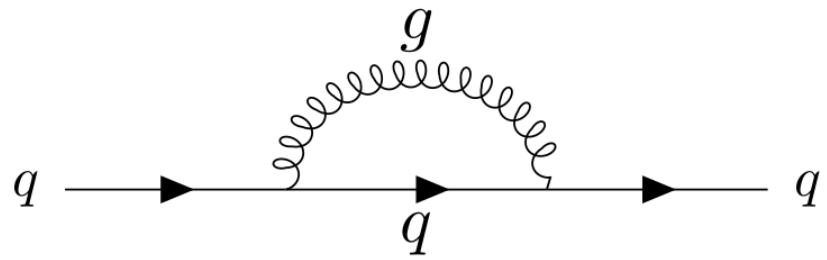

quark masses in QCD

renormalization of m_q

- definition of m_q depends on renormalization procedure

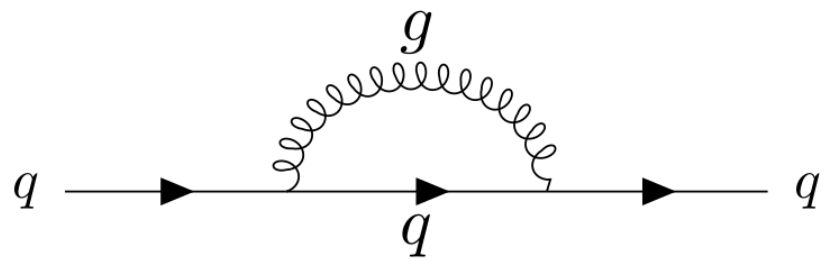

$$\frac{i}{\not{p} - m_0 - \delta m}$$

on-shell (pole) scheme $\rightarrow m_q^{\text{pole}}$

- fundamental ambiguity $\mathcal{O}(\Lambda_{\text{QCD}})$

quark masses in QCD

renormalization of m_q

- definition of m_q depends on renormalization procedure

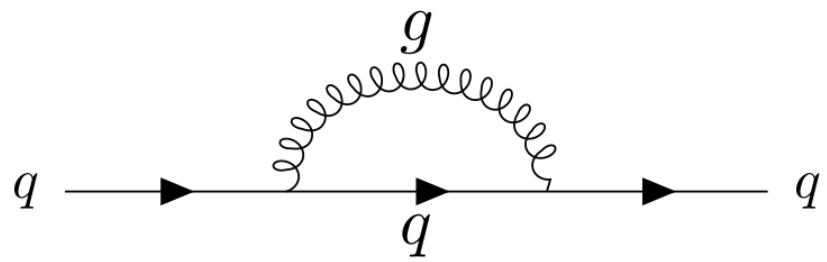

on-shell (pole) scheme $\rightarrow m_q^{\text{pole}}$

- fundamental ambiguity $\mathcal{O}(\Lambda_{\text{QCD}})$

short distance $(\overline{\text{MS}}) \rightarrow m_q(\mu_R)$

- running of m_q described by renormalization group equations

1. test of perturbative QCD
2. indirect search for new physics

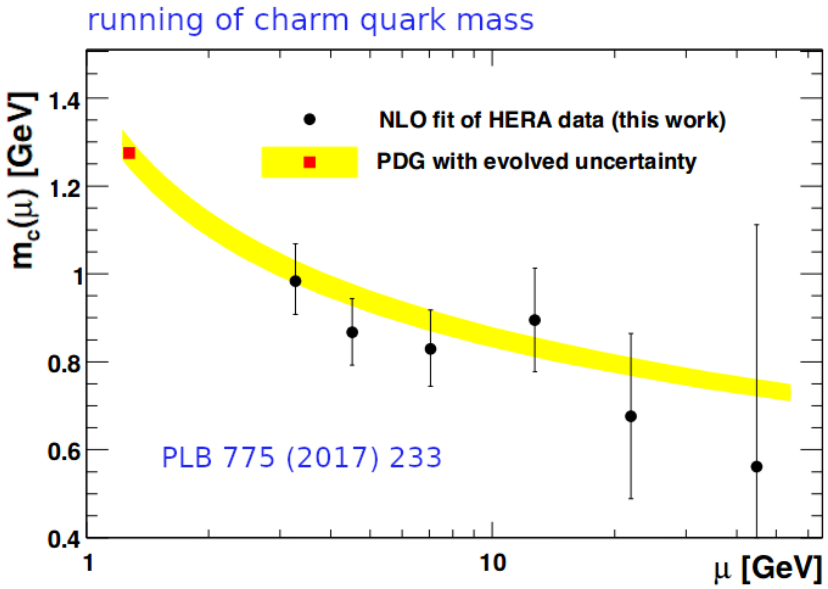

the role of the top quark mass

short lifetime $1/\Gamma_t \simeq 1/1.3\ \mathrm{GeV} < 1/\Lambda_{QCD}$

$\Rightarrow$ top quarks decay before hadronizing

- study properties of unconfined quark
- clear experimental signature

$\Uparrow$

large value of m_t

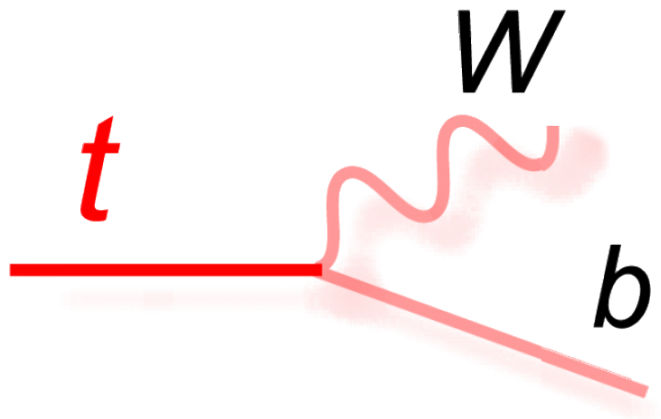

the role of the top quark mass

short lifetime $1/\Gamma_t \simeq 1/1.3\ \mathrm{GeV} < 1/\Lambda_{QCD}$

$\Rightarrow$ top quarks decay before hadronizing

- study properties of unconfined quark
- clear experimental signature

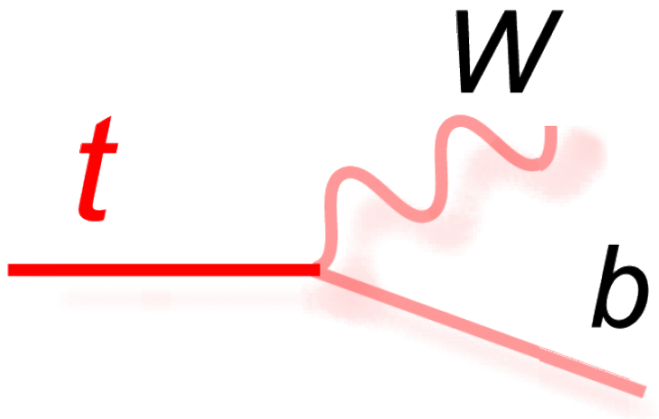

$\Uparrow$

large value of m_t $\Rightarrow$ natural hard scale for pQCD calculations

the role of the top quark mass

short lifetime $1/\Gamma_t \simeq 1/1.3\ \mathrm{GeV} < 1/\Lambda_{QCD}$

$\Rightarrow$ top quarks decay before hadronizing

- study properties of unconfined quark
- clear experimental signature

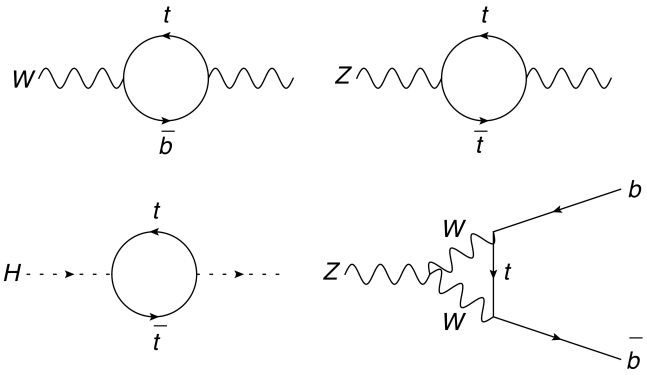

$\Uparrow$

large value of m_t $\Rightarrow$ natural hard scale for pQCD calculations

$\Downarrow$

large corrections to electroweak observables

- values of m_t, m_W, m_H can be determined simultaneously via electroweak fits
- comparison with direct measurements provides self-consistency test of SM

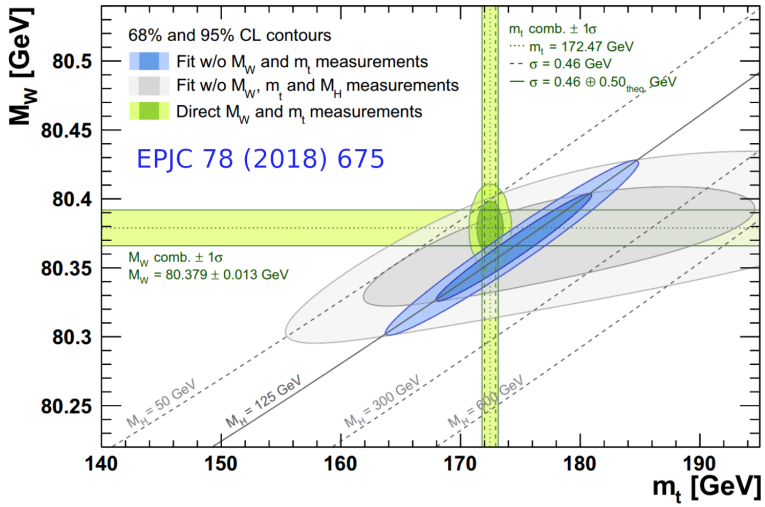

m_t and electroweak vacuum stability in the SM

RGE evolution of Higgs self-quartic coupling λ depends on values of m_t, α_S, and m_H

$\Rightarrow$ sign of λ at Planck scale determines stability of electroweak vacuum

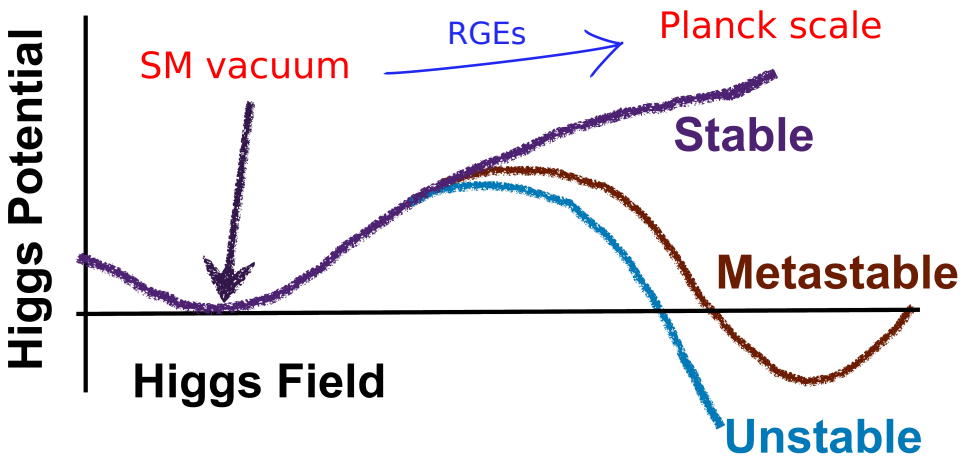

$\rightarrow$ need **precise measurements** of m_t, α_S, m_H

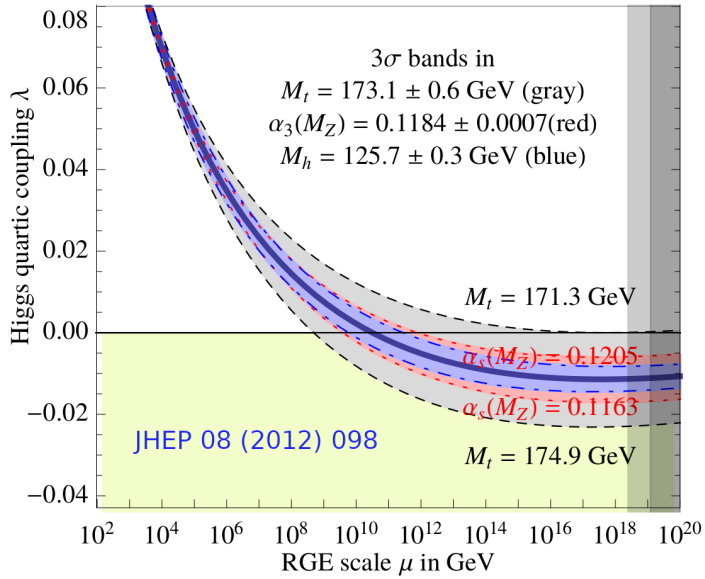

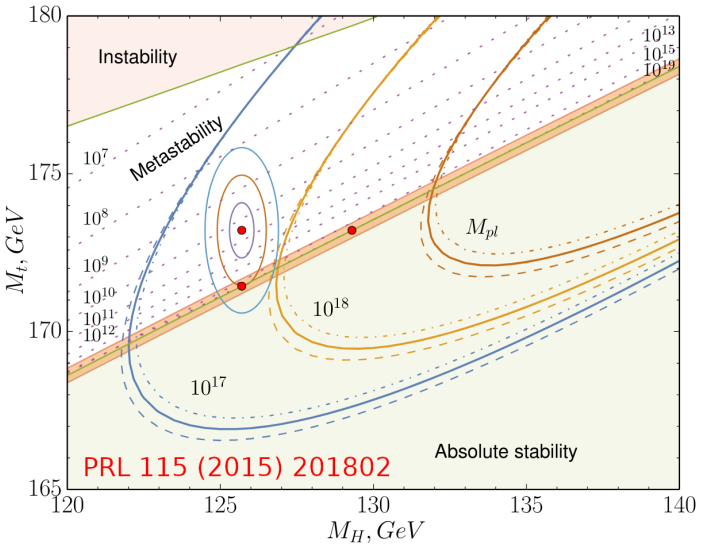

top quark production in proton-proton collisions

top quarks mainly produced in $\mathbf{t\bar{t}}$ **pairs**

1. gluon fusion $\rightarrow$ dominant at LHC
2. $q\bar{q}$ annihilation

calculations of $\sigma_{t\bar{t}}$

- available up to NNLO+NNLL precision
- comparison with measurement is test of pQCD

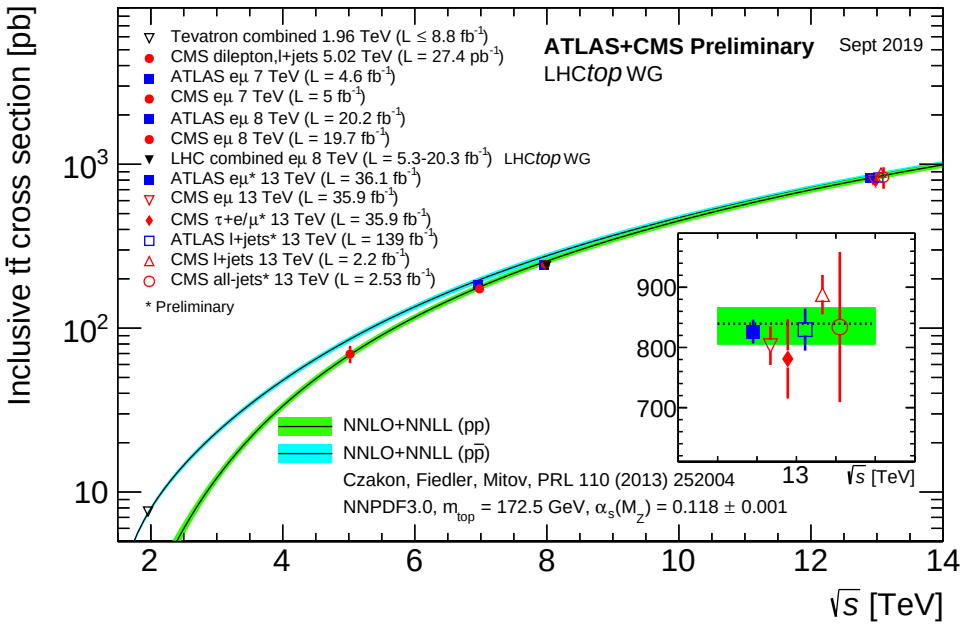

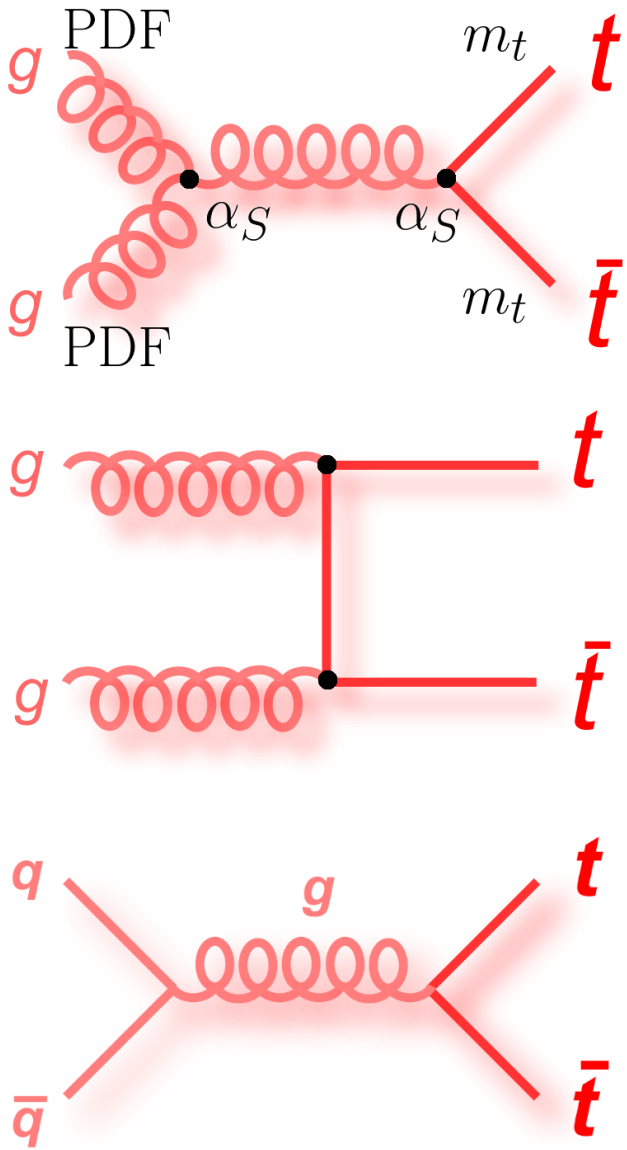

top quark final states

$t\bar{t}$ final states are classified based on decays of W bosons

1. $W \to \ell\,\nu_\ell$: leptonic
2. $W \to q\,\bar{q}'$: hadronic

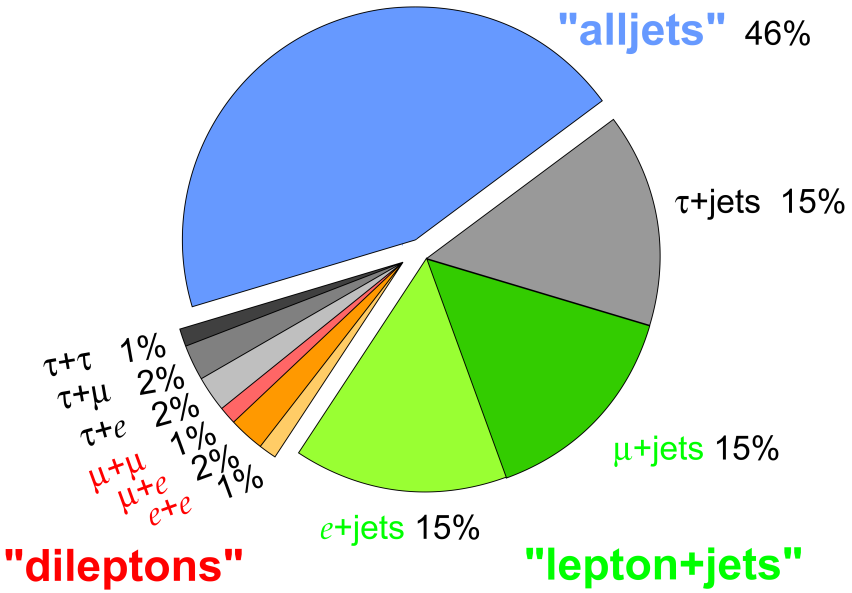

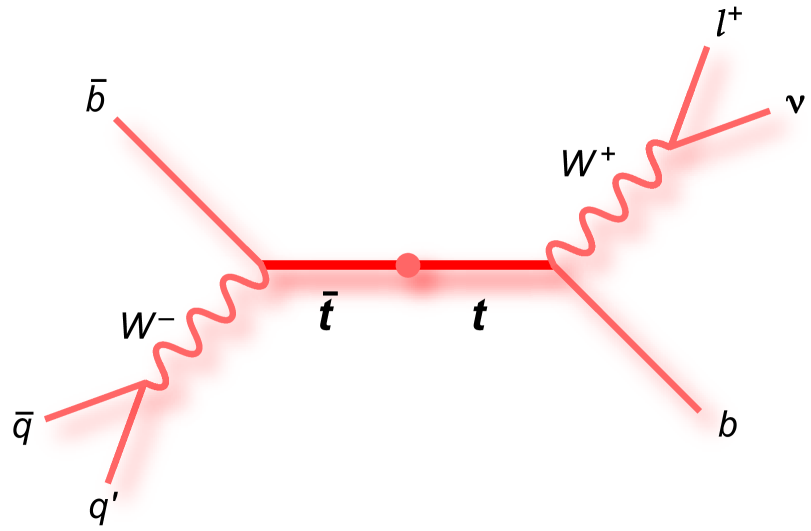

$t\bar{t}$ final states

- fully hadronic: large background
- dileptonic: clean signature
- semileptonic: intermediate properties

results obtained with in $e^{\mp}\mu^{\pm}$ channel
$\to$ highest signal purity

measuring m_t at a hadron collider

direct measurement: reconstruct invariant mass of top quark decay products

- compare to MC templates generated with different values of m_t

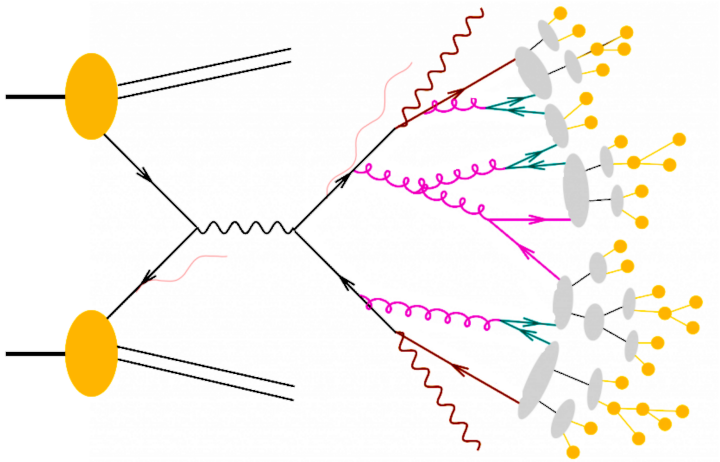

measuring m_{t} at a hadron collider

direct measurement: reconstruct invariant mass of top quark decay products

- compare to MC templates generated with different values of m_{t}

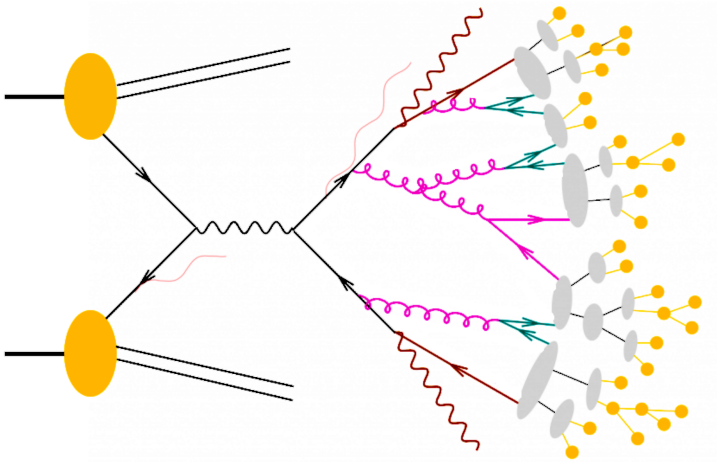

indirect determination: measure observable sensitive to m_{t} (e.g. $\sigma_{\mathrm{t\bar{t}}}$)

- compare measured $\sigma_{\mathrm{t\bar{t}}}$ to fixed-order calculations

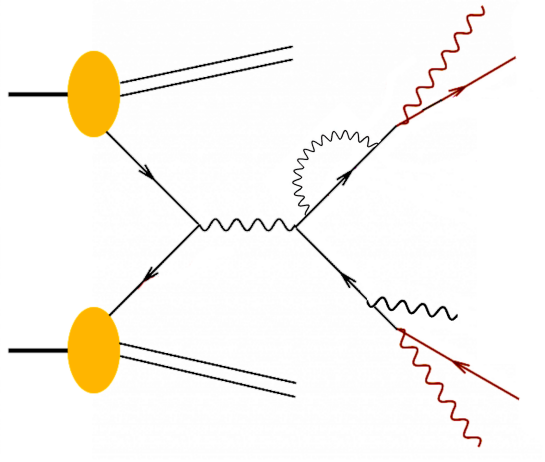

measuring m_{t} at a hadron collider

direct measurement: reconstruct invariant mass of top quark decay products

- compare to MC templates generated with different values of m_{t}

indirect determination: measure observable sensitive to m_{t} (e.g. $\sigma_{\mathrm{t\bar{t}}}$)

- compare measured $\sigma_{\mathrm{t\bar{t}}}$ to fixed-order calculations

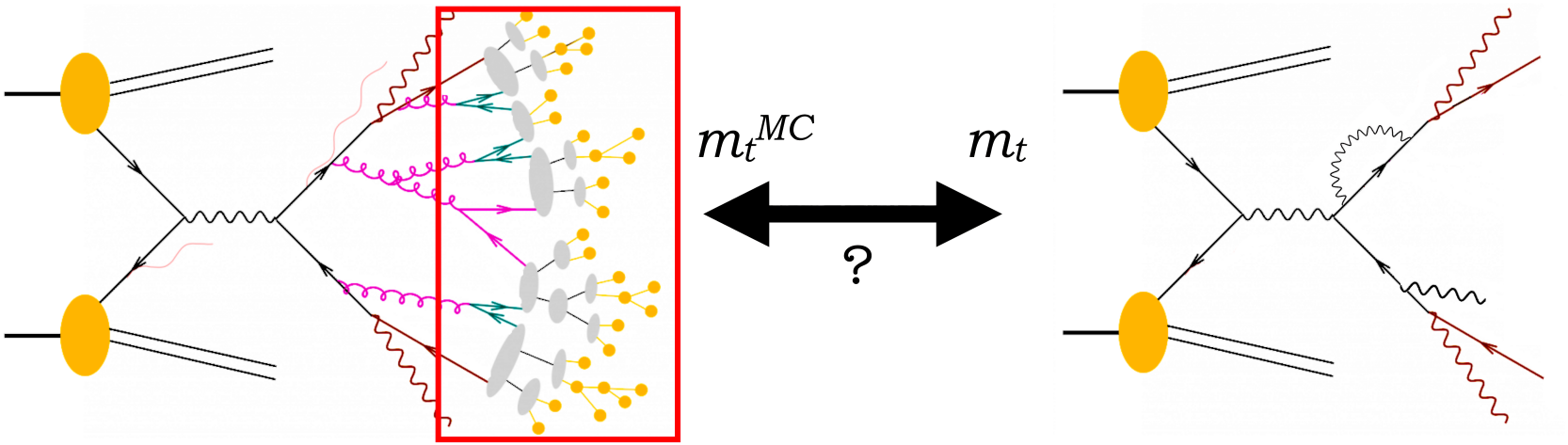

$$m_{\mathrm{t}}^{\mathrm{MC}} = m_{\mathrm{t}}^{\mathrm{pole}} \pm \Delta_{\mathrm{MC}}$$

$\rightarrow \Delta_{\mathrm{MC}}$ includes non-perturbative effects that are difficult to estimate

e.g. PRL 117 (2016) 232001

Measurement of the $\mathrm{t\bar{t}}$ production cross section at $\sqrt{s} = 13\,\mathrm{TeV}$

and extraction of the top quark mass and the strong coupling constant

the Large Hadron Collider

results obtained with pp collision data at $\sqrt{s} = 13\,\text{TeV}$ recorded by CMS in 2016

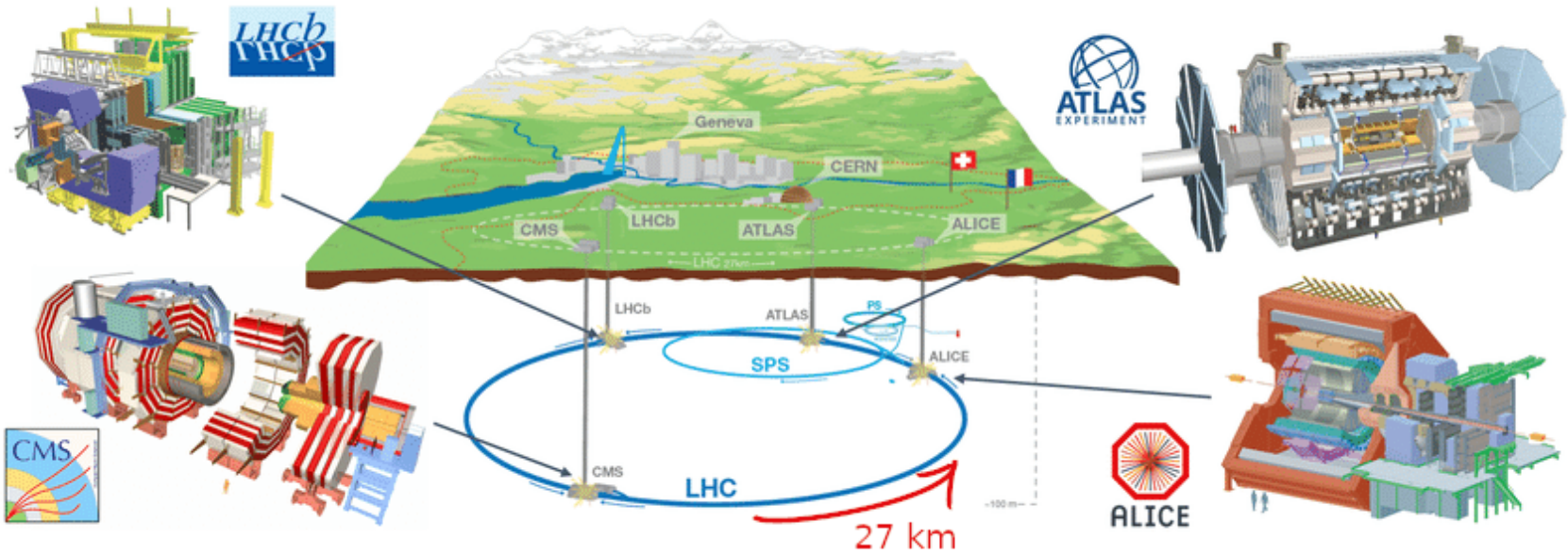

- superconducting accelerator at CERN laboratories in Geneva
- hadron-hadron collisions at the high-energy frontier, up to 13 TeV

the detector

- 3.8 T solenoidal magnetic field
- cylindrical layers around interaction point $\rightarrow$ particle discrimination

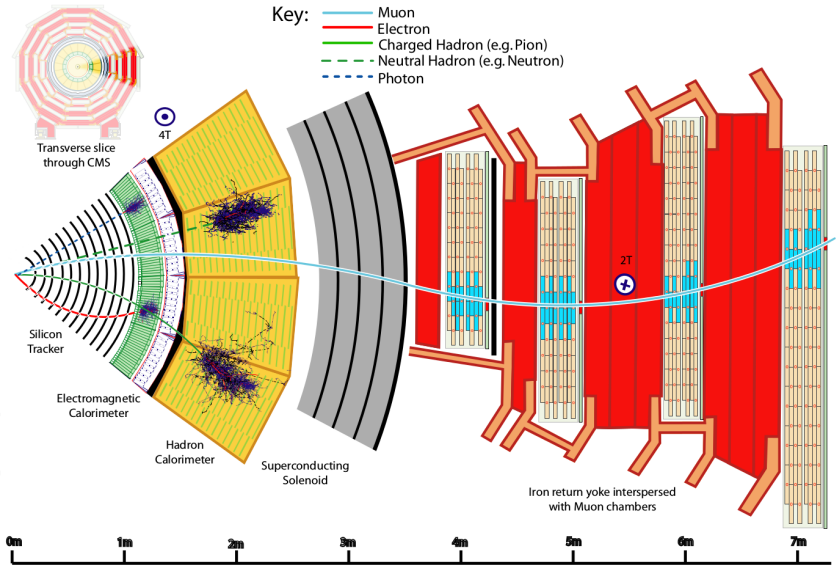

the CMS experiment at the LHC

the detector

- 3.8 T solenoidal magnetic field
- cylindrical layers around interaction point $\rightarrow$ particle discrimination

trigger system $\rightarrow$ select interesting events

1. L1: hardware $\rightarrow$ 100 kHz
2. high-level: software farm $\rightarrow \mathcal{O}(\mathrm{kHz})$

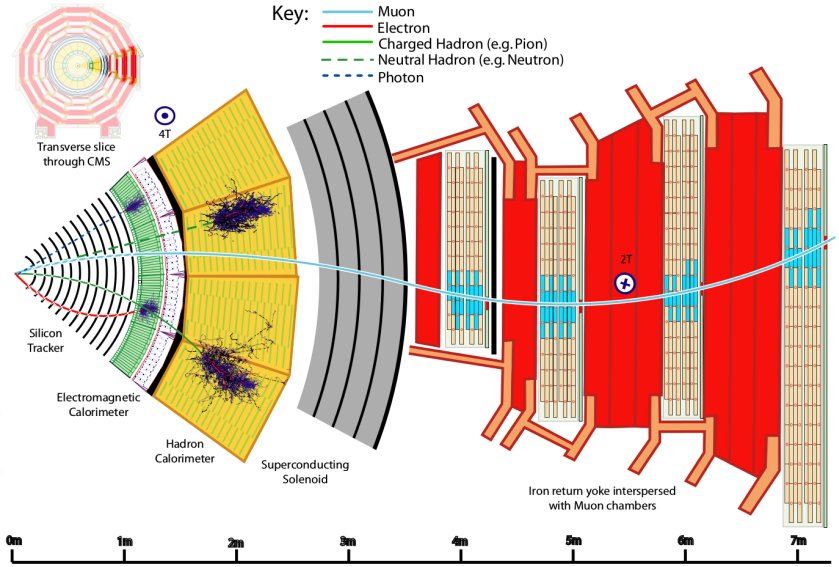

the CMS experiment at the LHC

the detector

- 3.8 T solenoidal magnetic field
- cylindrical layers around interaction point $\rightarrow$ particle discrimination

trigger system $\rightarrow$ select interesting events

1. L1: hardware $\rightarrow$ 100 kHz
2. high-level: software farm $\rightarrow \mathcal{O}(\mathrm{kHz})$

offline reconstruction

- Particle Flow (PF) algorithm
- PF candidates clustered in jets
- b-jets reconstructed exploiting long lifetime of B hadrons

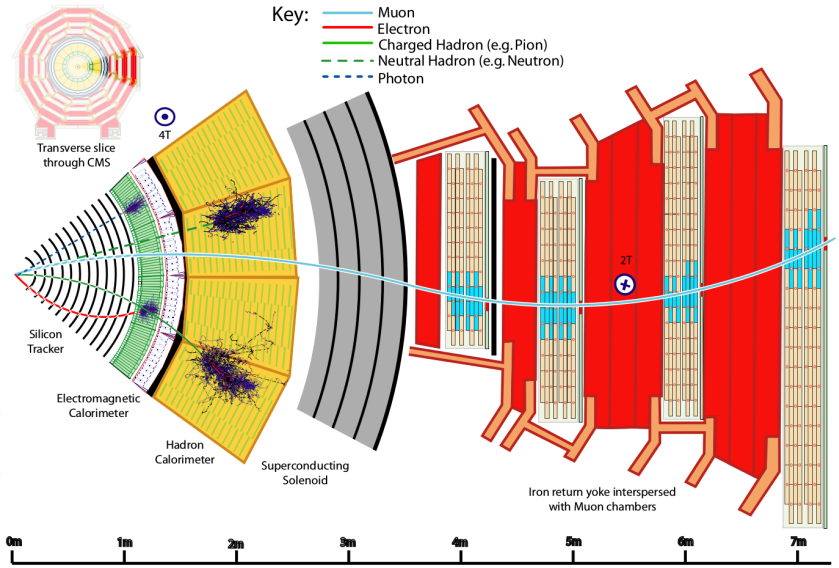

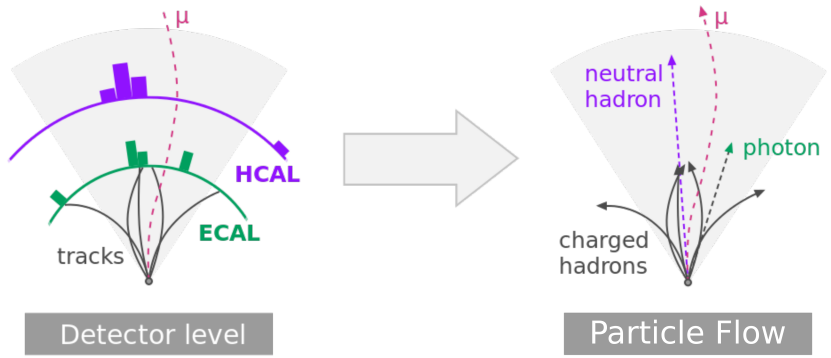

measurement of $\sigma_{t\bar{t}}$ in pp collisions at $\sqrt{s} = 13\,\text{TeV}$

- $\mathcal{L} = 35.9\ \text{fb}^{-1}$, $\sqrt{s} = 13\,\text{TeV}$
- $t\bar{t} \to e^{\mp}\mu^{\pm}b\bar{b}\,\nu\bar{\nu}$

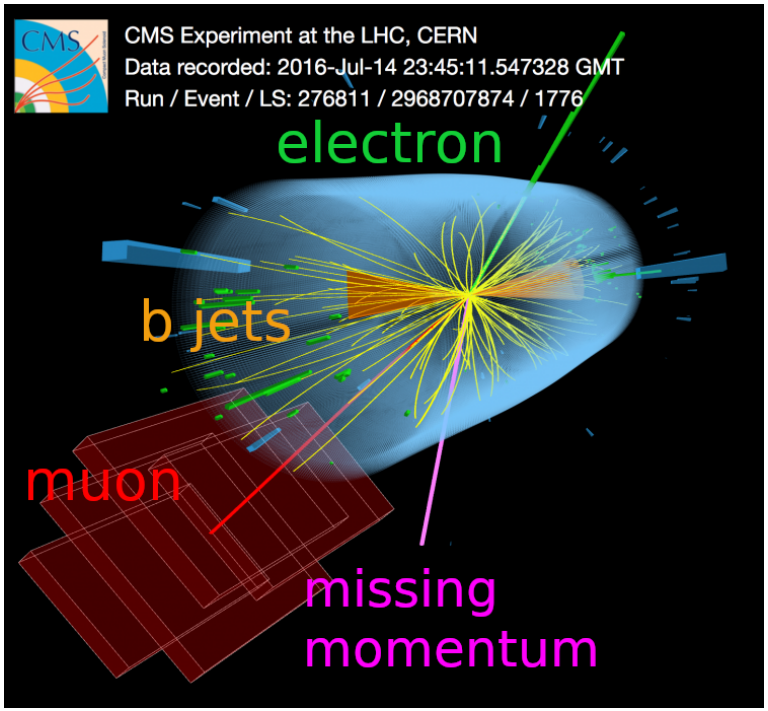

- missing p_T: escaping neutrinos
- possible additional jets

measurement of $\sigma_{t\bar{t}}$ in pp collisions at $\sqrt{s} = 13\,\text{TeV}$

- $\mathcal{L} = 35.9\ \text{fb}^{-1}$, $\sqrt{s} = 13\,\text{TeV}$
- $t\bar{t} \to e^{\mp}\mu^{\pm} b\bar{b}\,\nu\bar{\nu}$

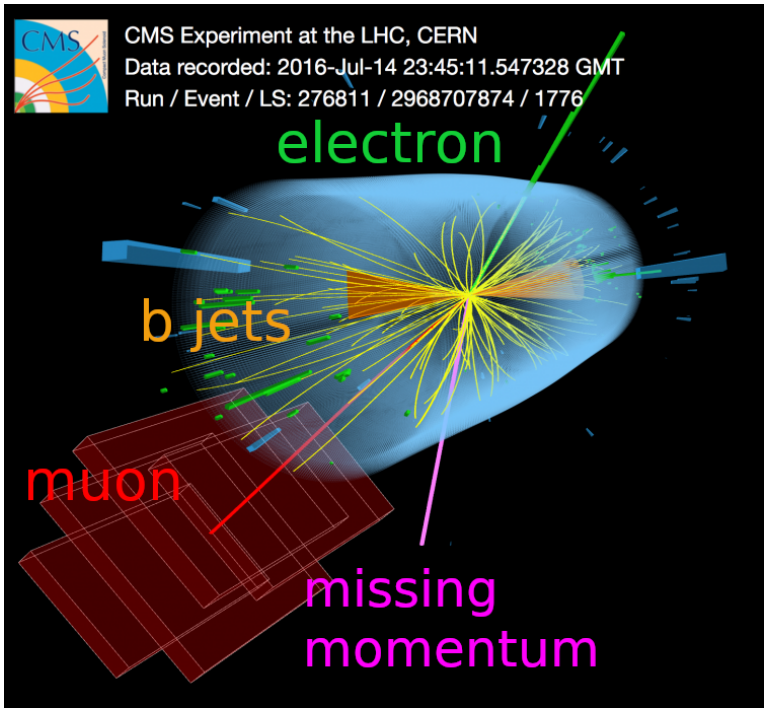

- missing p_T: escaping neutrinos
- possible additional jets

visible phase space

1. detector geometry
2. selection of final-state objects

$$\sigma_{t\bar{t}}^{\text{vis}} = \frac{N_{\text{data}} - N_{\text{bkg}}}{\epsilon_{\text{sel}} \cdot \mathcal{L}_{\text{int}}}$$

$$\to \sigma_{t\bar{t}} = \frac{\sigma_{t\bar{t}}^{\text{vis}}}{A_{\text{sel}} \cdot \text{BR}(t\bar{t} \to e^{\mp}\mu^{\pm})}$$

measurement of $\sigma_{t\bar{t}}$ in pp collisions at $\sqrt{s} = 13\,\text{TeV}$

- $\mathcal{L} = 35.9\ \text{fb}^{-1}$, $\sqrt{s} = 13\,\text{TeV}$
- $t\bar{t} \to e^{\mp}\mu^{\pm} b\bar{b}\,\nu\bar{\nu}$

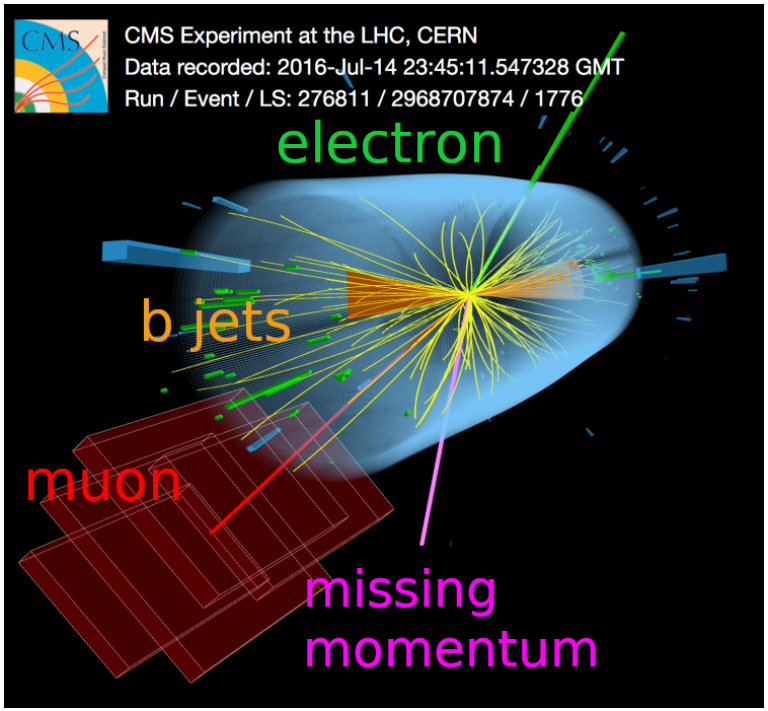

- missing p_T: escaping neutrinos
- possible additional jets

visible phase space

1. detector geometry
2. selection of final-state objects

$$\sigma_{t\bar{t}}^{\text{vis}} = \frac{N_{\text{data}} - N_{\text{bkg}}}{\epsilon_{\text{sel}} \cdot \mathcal{L}_{\text{int}}}$$

$$\to\ \sigma_{t\bar{t}} = \frac{\sigma_{t\bar{t}}^{\text{vis}}}{A_{\text{sel}} \cdot \text{BR}(t\bar{t} \to e^{\mp}\mu^{\pm})}$$

selection acceptance A_{sel}:

- determined from simulation
- depends on assumed m_t^{MC}

$\to$ dependence mitigated via **simultaneous measurement of $\sigma_{t\bar{t}}$ and m_t^{MC}**

simultaneous fit of $\sigma_{t\bar{t}}$ and m_t^{MC}

binned maximum-likelihood fit to multi-differential distributions

$$L(\sigma_{t\bar{t}}, m_t^{MC}, \vec{\lambda}) = \underbrace{\prod_i \frac{e^{-\nu_i}\nu_i^{n_i}}{n_i!}}_{\text{Poisson}} \underbrace{\prod_m \pi_m(\lambda_m)}_{\text{priors}}$$

$$\nu_i = \underbrace{s_i(\sigma_{t\bar{t}}, m_t^{MC}, \vec{\lambda})}_{\text{signal}} + \underbrace{\sum_j b_i^j(\vec{\lambda})}_{\text{backgrounds}}$$

- systematic uncertainties ($\vec{\lambda}$) constrained using data
- signal and background contributions measured simultaneously

multi-differential distributions used in the fit

0 b-tags: 0,1,2,3 additional jets → jet p_T distribution: constrain jet energy scale

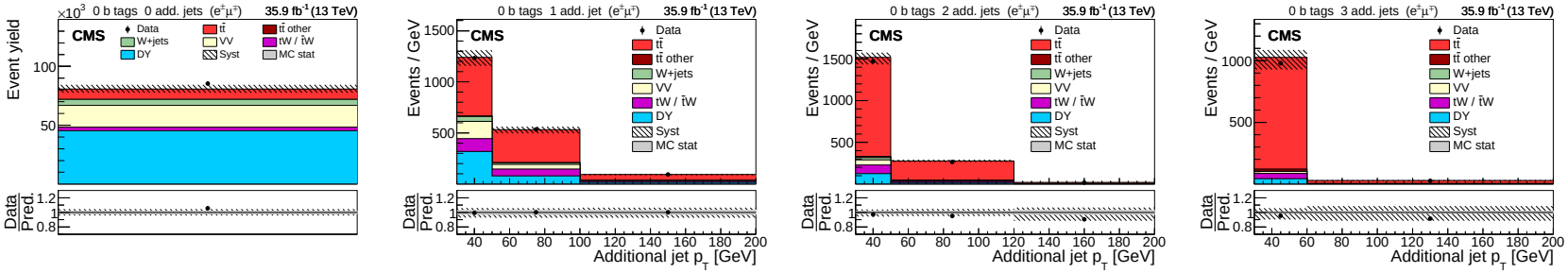

1 b-tag: 0,1,2,3 additional jets → $m_{\ell b}^{\min}$ distribution: sensitive to m_t^{MC}

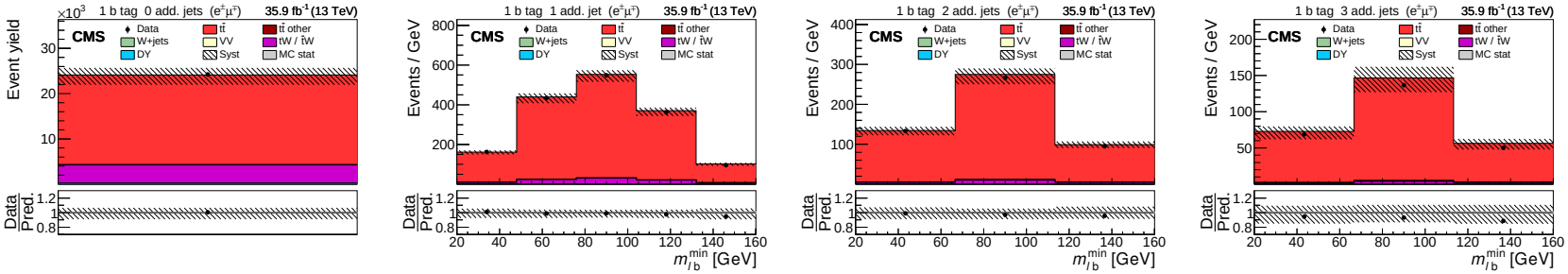

2 b-tags: 0,1,2,3 additional jets → $m_{\ell b}^{\min}$ distribution: sensitive to m_t^{MC}

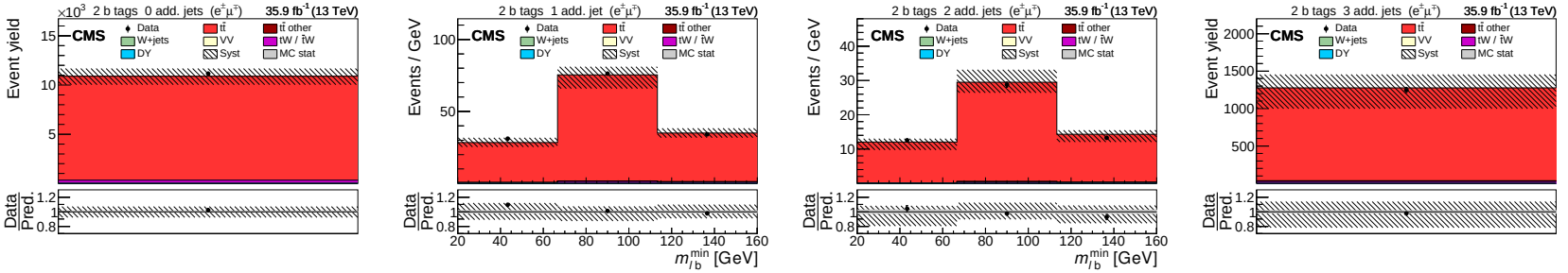

multi-differential distributions used in the fit

0 b-tags: 0,1,2,3 additional jets → jet p_T distribution: constrain jet energy scale

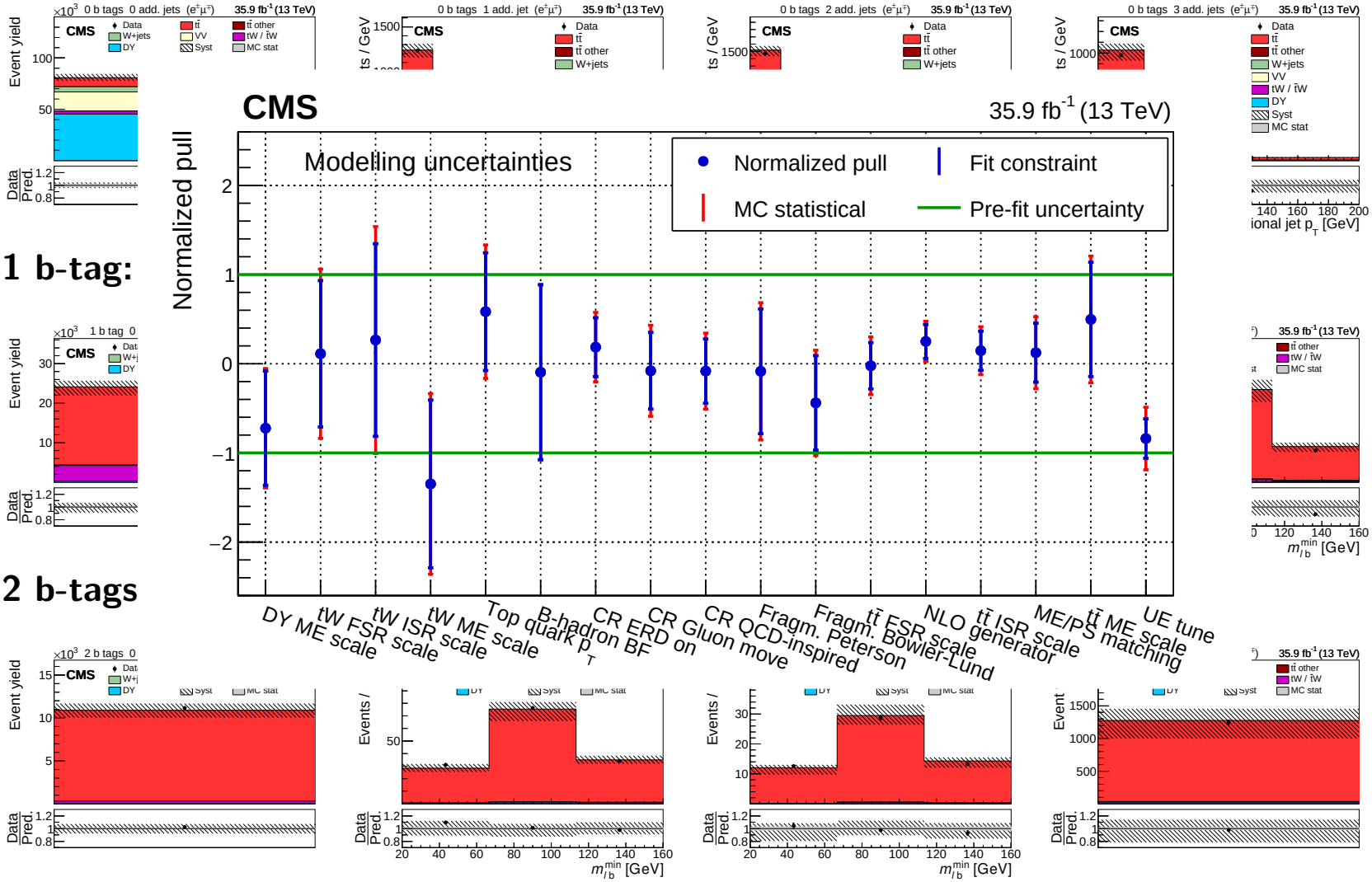

results for $\sigma_{t\bar{t}}$ at $\sqrt{s} = 13\,\text{TeV}$

$$\sigma_{t\bar{t}} = 815 \pm 2\,(\text{stat}) \pm 29\,(\text{syst}) \pm 20\,(\text{lum})\,\text{pb}$$

- total uncertainty: 4.3%
- among most precise results in CMS

main sources of uncertainty

- integrated luminosity (2.5%)
- lepton identification (2.2%)

} normalization

→ good agreement with theoretical prediction at NNLO+NNLL (Top++)

$$\sigma^{\text{th}}_{t\bar{t}} = 832\,^{+20}_{-29}\,(\text{scale}) \pm 35\,(\text{PDF} + \alpha_S)\,\text{pb}$$

Source	Uncertainty [%]
Trigger	0.4
Lepton ident./isolation	2.2
Muon momentum scale	0.2
Electron momentum scale	0.2
Jet energy scale	0.7
Jet energy resolution	0.5
b tagging	0.3
Pileup	0.3
$t\bar{t}$ ME scale	0.5
tW ME scale	0.7
DY ME scale	0.2
NLO generator	1.2
PDF	1.1
m_t^{MC}	0.4
Top quark p_T	0.5
ME/PS matching	0.2
UE tune	0.3
$t\bar{t}$ ISR scale	0.4
tW ISR scale	0.4
$t\bar{t}$ FSR scale	1.1
tW FSR scale	0.2
b quark fragmentation	1.0
b hadron BF	0.2
Colour reconnection	0.4
DY background	0.8
tW background	1.1
Diboson background	0.3
W+jets background	0.3
$t\bar{t}$ background	0.2
Statistical	0.2
Integrated luminosity	2.5
MC statistical	1.2
Total $\sigma^{vis}_{t\bar{t}}$ uncertainty	4.2
Extrapolation uncertainties	
$t\bar{t}$ ME scale	$\mp^{0.4}_{<0.1}$
PDF	$\pm^{0.8}_{0.6}$
Top quark p_T	$\pm^{0.2}_{0.3}$
$t\bar{t}$ ISR scale	$\mp^{0.2}_{<0.1}$
$t\bar{t}$ FSR scale	± 0.1
UE tune	<0.1
m_t^{MC}	$\mp^{0.2}_{0.3}$
Total $\sigma_{t\bar{t}}$ uncertainty	$^{+4.3}_{-4.2}$

results for $m_{\mathrm{t}}^{\mathrm{MC}}$

$$m_{\mathrm{t}}^{\mathrm{MC}} = 172.33 \pm 0.14\,(\mathrm{stat}) \pm^{0.66}_{0.72}\,(\mathrm{syst})\,\mathrm{GeV}$$

- total uncertainty: 0.41%
- correlation with $\sigma_{\mathrm{t\bar{t}}}$: 12%

main sources of uncertainty

- jet energy scale (0.57 GeV)
- MC statistics (0.36 MeV)

} $m_{\ell\mathrm{b}}^{\mathrm{min}}$ shape

$\rightarrow$ similar precision as dedicated analyses in ℓ+jets and fully-hadronic channels

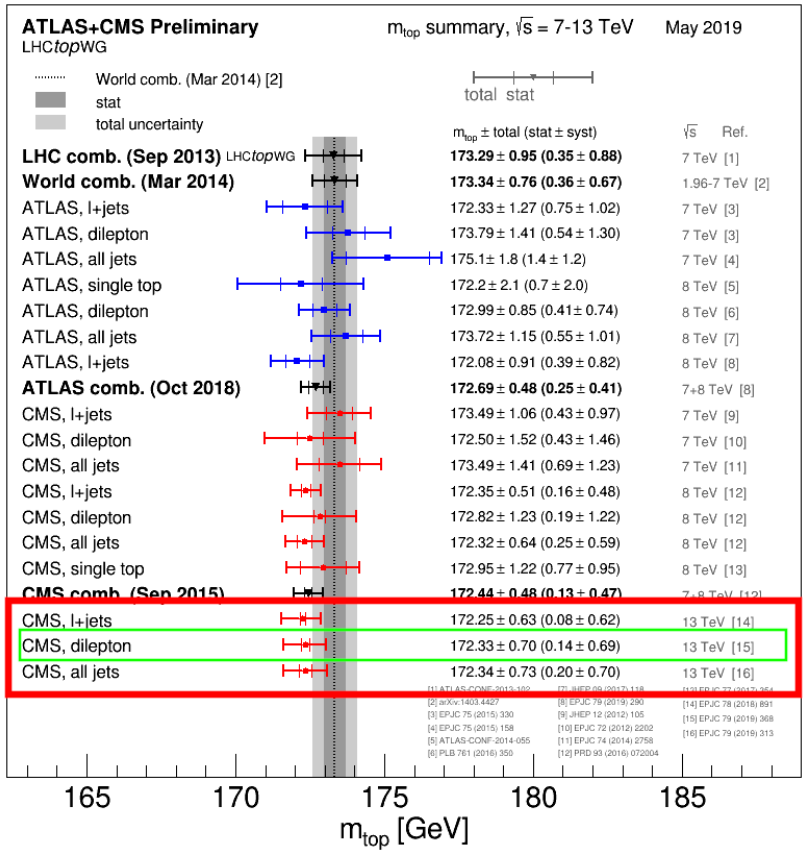

extraction of m_t and α_S from inclusive $\sigma_{t\bar{t}}$

values of m_t and α_S extracted by comparing measured $\sigma_{t\bar{t}}$ to fixed-order calculations

- Hathor calculations at NNLO
- m_t defined in $\overline{\text{MS}}$ scheme
  $\rightarrow$ faster perturbative convergence

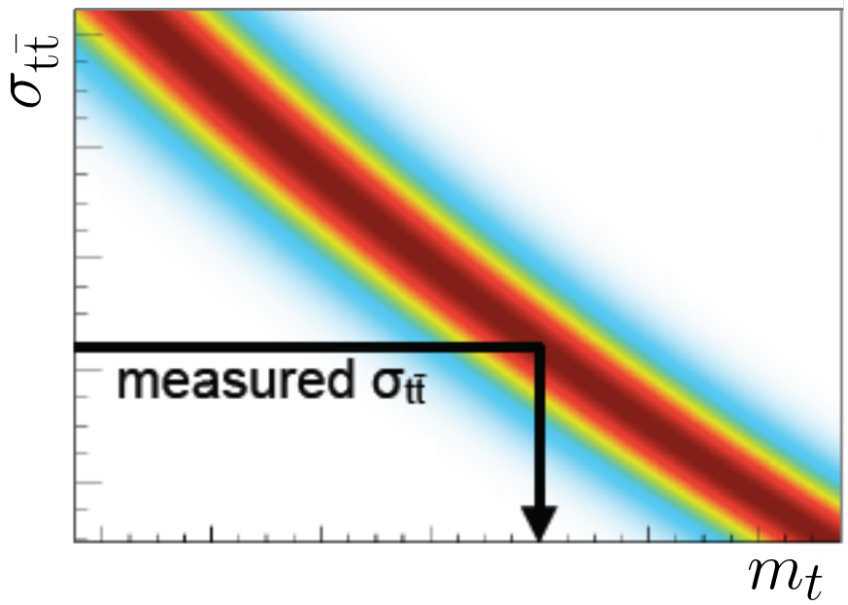

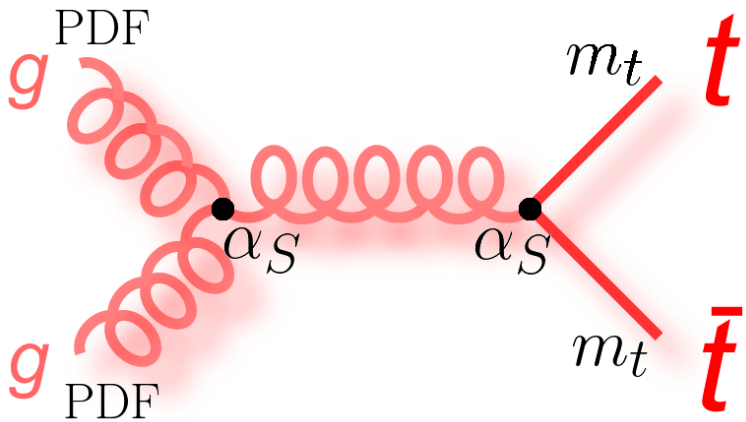

α_S and m_t cannot be determined simultaneously from measured $\sigma_{t\bar{t}}$

$\Rightarrow$ when extracting one, an assumption on the other (and PDFs) must be made

extraction of $\alpha_S(m_Z)$ from $\sigma_{t\bar{t}}$

$\alpha_S(m_Z)$ determined via χ^2 **fit** of theoretical predictions to measured $\sigma_{t\bar{t}}$

- value of $\alpha_S(m_Z)$ consistently changed in calculation and PDFs
- several NNLO PDF sets considered
- m_t fixed to the value in PDF

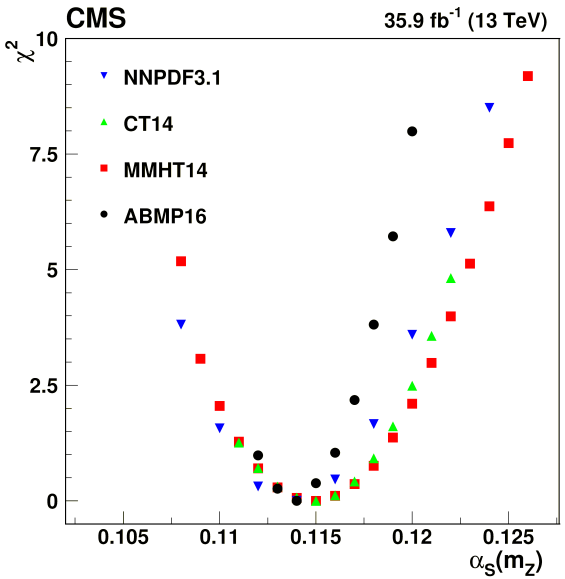

extraction of $\alpha_S(m_Z)$ from $\sigma_{t\bar{t}}$

$\alpha_S(m_Z)$ determined via χ^2 **fit** of theoretical predictions to measured $\sigma_{t\bar{t}}$

- value of $\alpha_S(m_Z)$ consistently changed in calculation and PDFs
- several NNLO PDF sets considered
- m_t fixed to the value in PDF

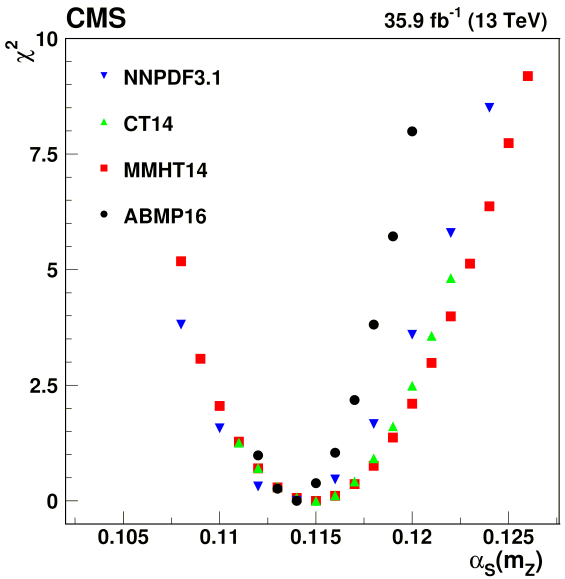

results

- precision of order 2-3%
- good agreement between different PDFs

$$\alpha_S(m_Z) = 0.1139\ ^{+0.0027}_{-0.0023} \quad \text{(ABMP16)}$$

→ **most precise NNLO result at hadron collider**, to date

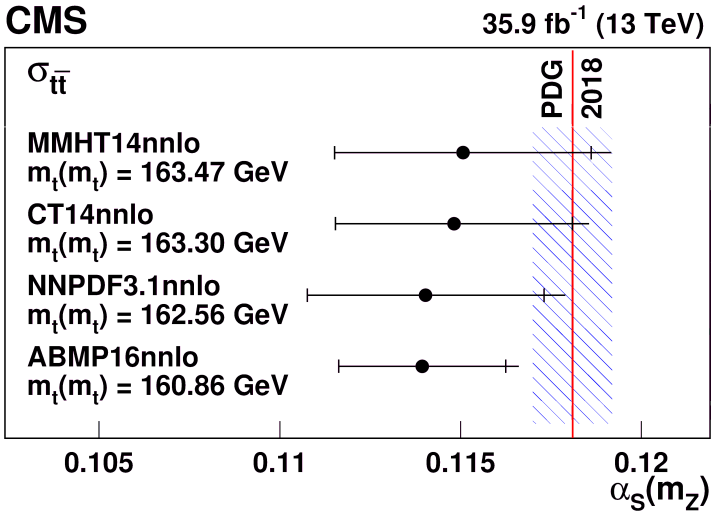

extraction of $m_t(m_t)$ from $\sigma_{t\bar{t}}$

- same procedure used to extract top mass in $\overline{\mathrm{MS}}$ scheme, $m_t(m_t)$
- $\alpha_S(M_Z)$ fixed to values in PDF

results

- uncertainty $\simeq 1.2\%$

$$m_t(m_t) = 161.6\ ^{+1.6}_{-1.9}\ \text{GeV}\ (\text{ABMP16})$$

$\rightarrow$ **first consistent and most precise determination of $m_t(m_t)$**, to date

- lower m_t result with ABMP16 due to lower $\alpha_S(m_Z)$ in PDFs
- linear dependence between α_S and m_t

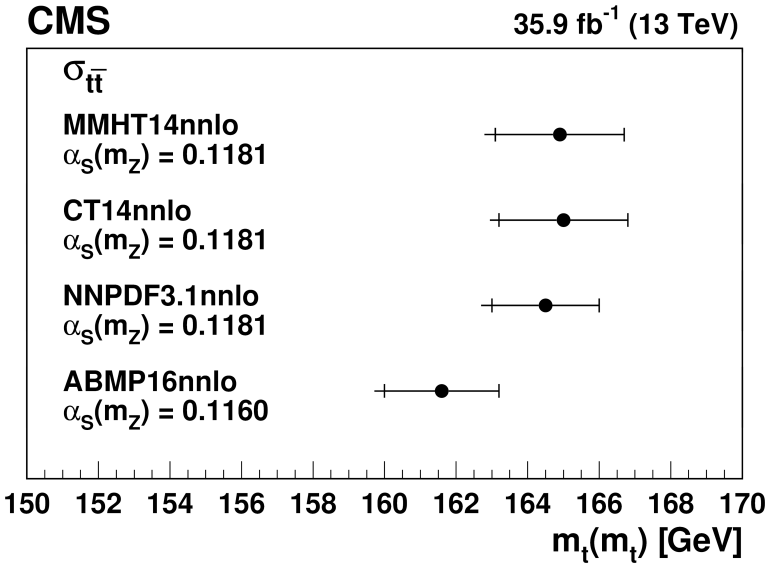

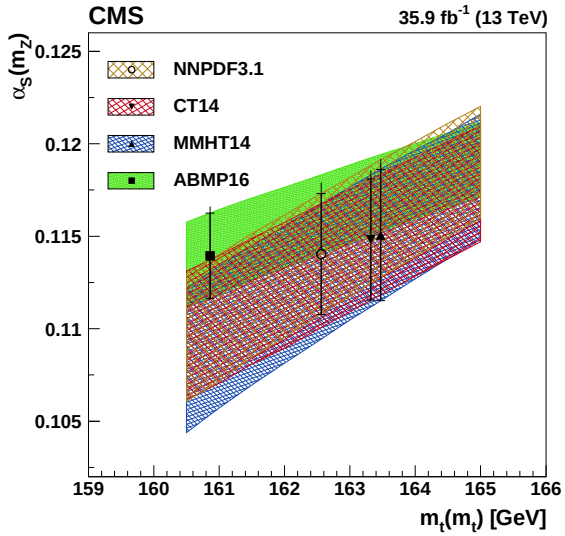

First measurement of the running of the top quark mass

measurement of the running of m_t

example: **running of α_S**

- measure observable sensitive of α_S as a function of energy scale Q
- extract α_S in bins of Q
- compare $\alpha_S(Q)$ to RGE prediction

$\rightarrow$ same procedure can be used to extract the running of m_t

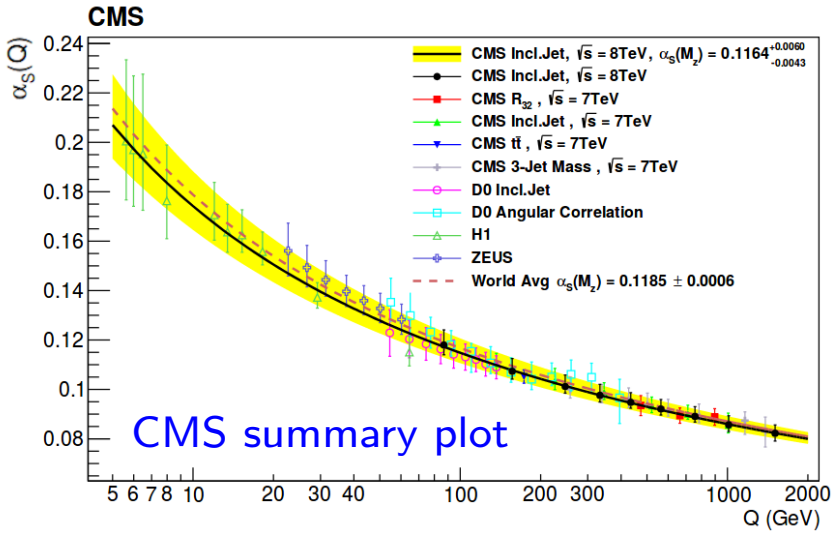

measurement of the running of m_t

example: **running of α_S**

- measure observable sensitive of α_S as a function of energy scale Q
- extract α_S in bins of Q
- compare $\alpha_S(Q)$ to RGE prediction

$\rightarrow$ same procedure can be used to extract the running of m_t

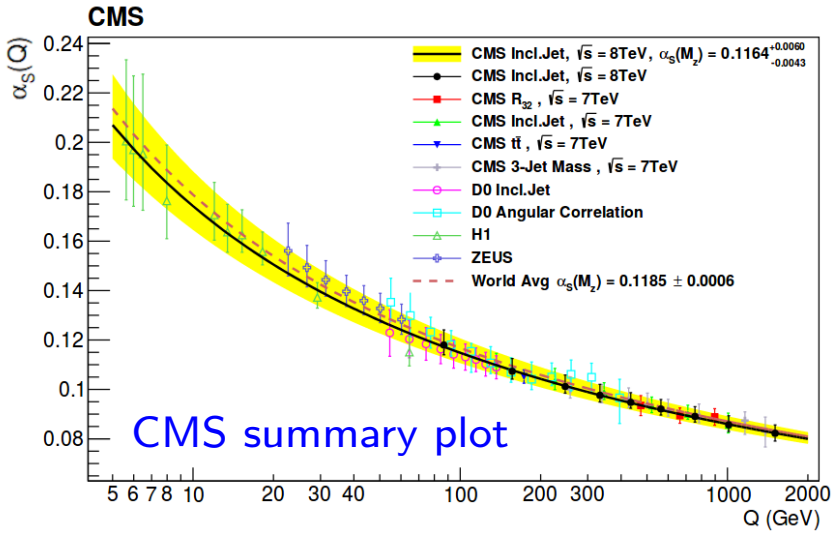

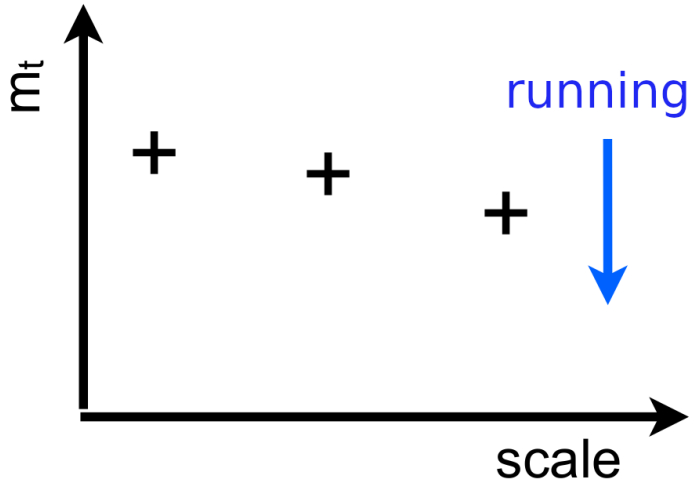

running of m_t: measure $m_t(\mu)$ as a function of the energy scale $\mu > m_t$

- observable $= \sigma_{t\bar{t}}$
- $Q \rightarrow \mu = m_{t\bar{t}}$

$\Rightarrow d\sigma_{t\bar{t}}/dm_{t\bar{t}}$

$\rightarrow$ natural extension of inclusive analysis

$m_{t\bar{t}}$ reconstruction

- kinematic reconstruction of $m_{t\bar{t}}^{reco}$
  1. efficiency $\simeq$ 90%
  2. resolution $\simeq$ 13%
- $m_{t\bar{t}}^{reco}$ unfolded to parton-level $m_{t\bar{t}}$

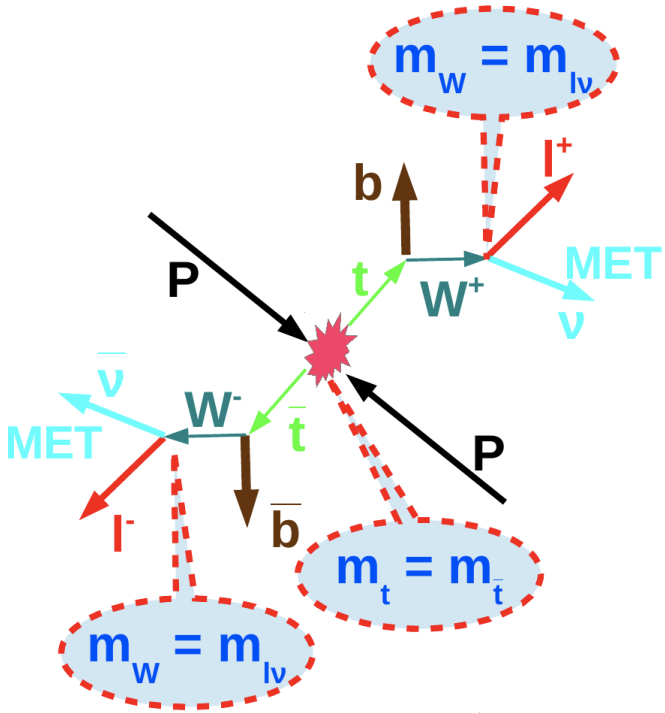

$m_{\mathrm{t\bar{t}}}$ reconstruction

- kinematic reconstruction of $m_{\mathrm{t\bar{t}}}^{\mathrm{reco}}$
  1. efficiency $\simeq 90\%$
  2. resolution $\simeq 13\%$
- $m_{\mathrm{t\bar{t}}}^{\mathrm{reco}}$ unfolded to parton-level $m_{\mathrm{t\bar{t}}}$

solving the unfolding problem

estimate true spectrum using quantities measured in the detector

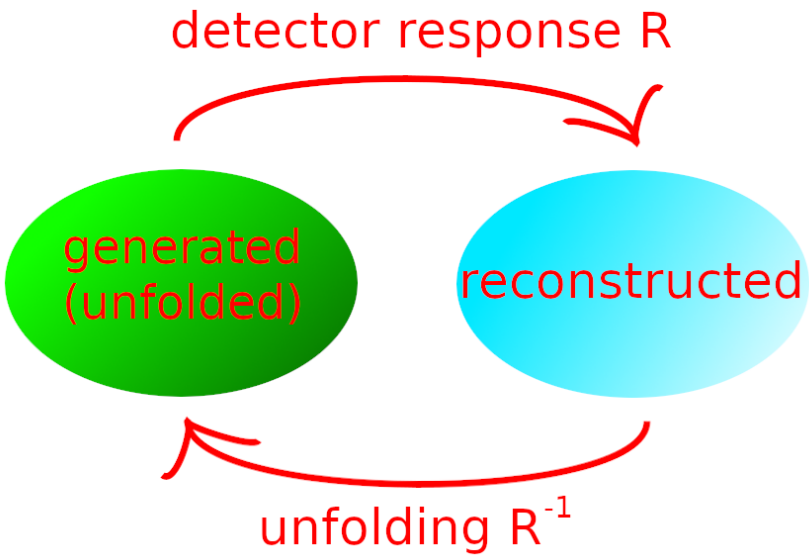

measurement of $\mathrm{d}\sigma_{\mathrm{t\bar{t}}}/\mathrm{d}m_{\mathrm{t\bar{t}}}$ at $\sqrt{s} = 13\,\mathrm{TeV}$

$m_{\mathrm{t\bar{t}}}$ reconstruction

- kinematic reconstruction of $m_{\mathrm{t\bar{t}}}^{\mathrm{reco}}$
  1. efficiency $\simeq 90\%$
  2. resolution $\simeq 13\%$
- $m_{\mathrm{t\bar{t}}}^{\mathrm{reco}}$ unfolded to parton-level $m_{\mathrm{t\bar{t}}}$

solving the unfolding problem

estimate true spectrum using quantities measured in the detector

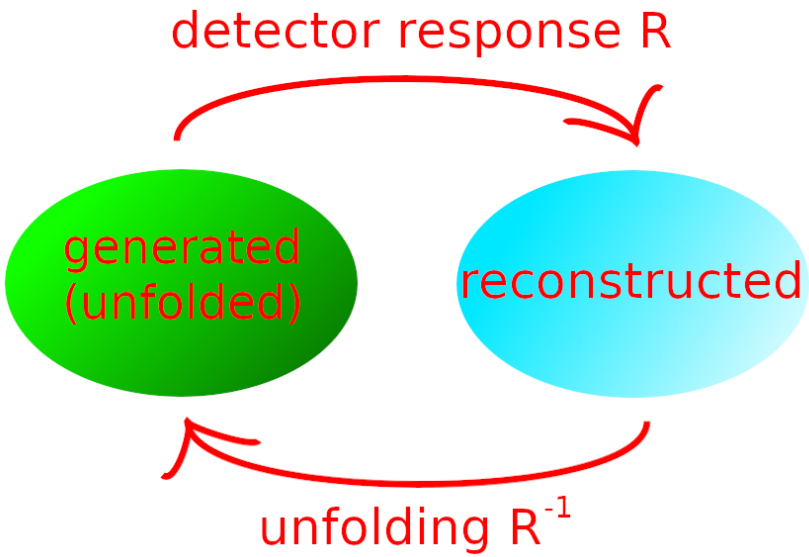

this analysis: **maximum-likelihood** method

- simultaneous fit of signal and background contributions
- systematic uncertainties constrained in the visible phase space

$$\mathcal{L}(\text{data} \mid \underbrace{\mathrm{d}\sigma_{\mathrm{t\bar{t}}}/\mathrm{d}m_{\mathrm{t\bar{t}}}}, R\,)$$

determined directly at parton level

implementation of the unfolding

- $\mathrm{t\bar{t}}$ simulation split into 4 subsamples in bins of parton-level $m_{\mathrm{t\bar{t}}}$
- each subsample treated as an independent signal $\rightarrow \mathrm{d}\sigma_{\mathrm{t\bar{t}}}/\mathrm{d}m_{\mathrm{t\bar{t}}}$

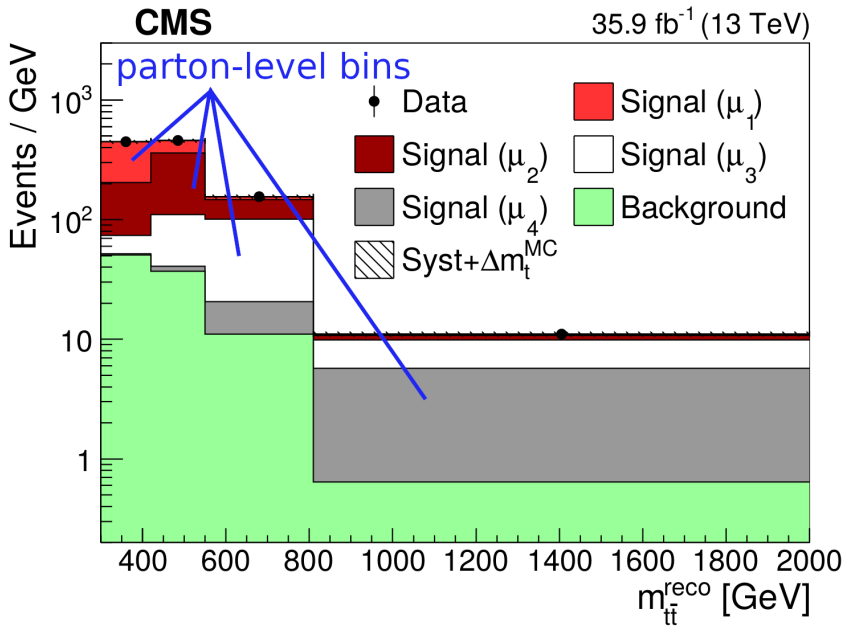

bin	range [GeV]	μ_k [GeV]
1	< 420	384
2	420-550	476
3	550-810	644
4	> 810	1024

implementation of the unfolding

- $\mathrm{t\bar{t}}$ simulation split into 4 subsamples in bins of parton-level $m_{\mathrm{t\bar{t}}}$
- each subsample treated as an independent signal $\rightarrow \mathrm{d}\sigma_{\mathrm{t\bar{t}}}/\mathrm{d}m_{\mathrm{t\bar{t}}}$

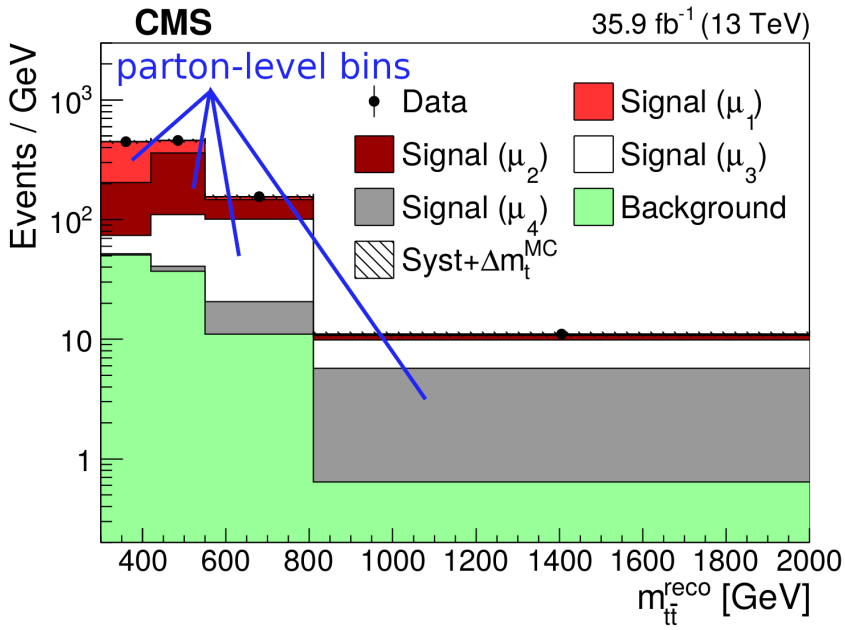

choice of the scale

- μ_k = centre-of-gravity of $m_{\mathrm{t\bar{t}}}$
- final result does not depend on exact definition of μ_k

bin	range [GeV]	μ_k [GeV]
1	< 420	**384**
2	420-550	**476**
3	550-810	**644**
4	> 810	**1024**

result for $\mathrm{d}\sigma_{\mathrm{t\bar{t}}}/\mathrm{d}m_{\mathrm{t\bar{t}}}$ and extraction of $m_{\mathrm{t}}(\mu)$

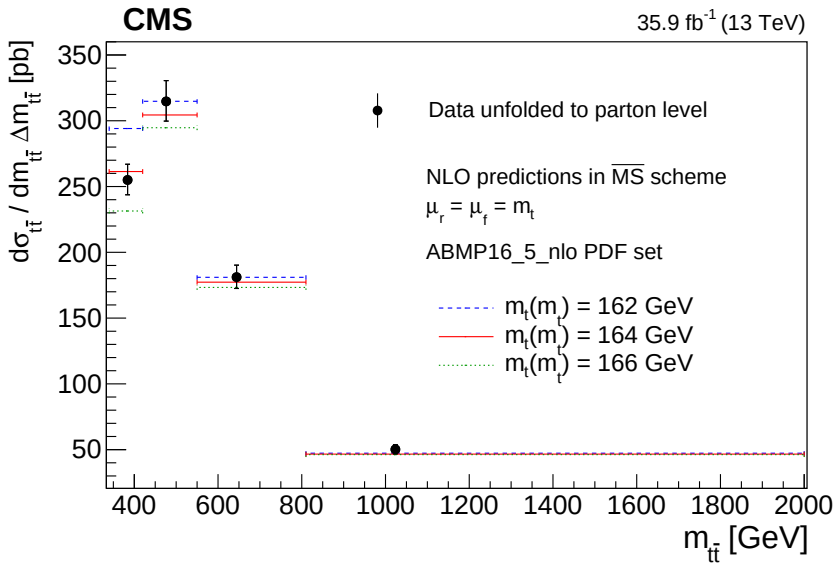

NLO predictions obtained with version of MCFM where m_{t} is treated in $\overline{\mathrm{MS}}$ scheme
$\rightarrow$ EPJC 74 (2014) 3167

- first top physics result obtained with rigorous likelihood-based unfolding
- **significantly improved precision** compared to other methods

result for $\mathrm{d}\sigma_{\mathrm{t\bar{t}}}/\mathrm{d}m_{\mathrm{t\bar{t}}}$ and extraction of $m_{\mathrm{t}}(\mu)$

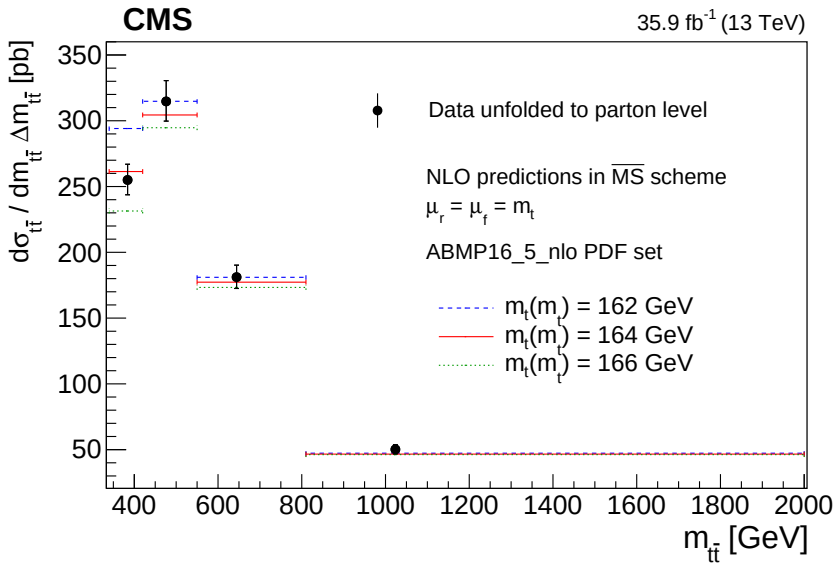

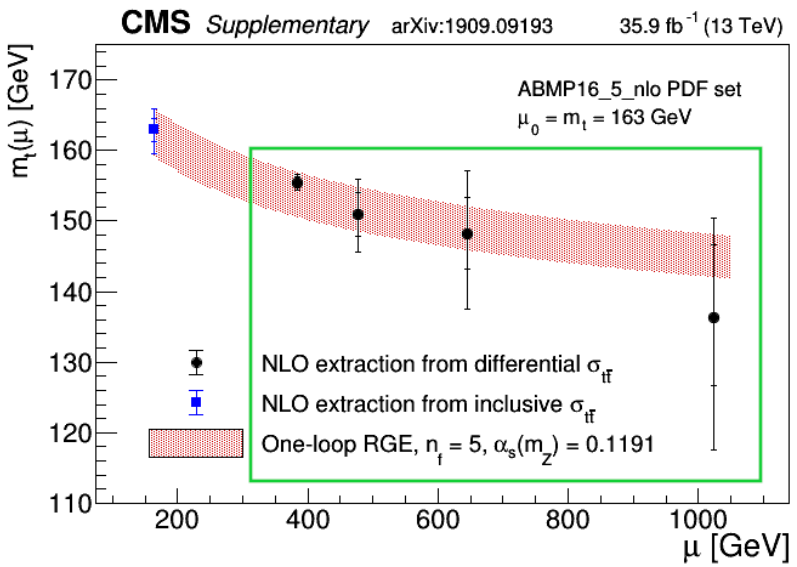

NLO predictions obtained with version of MCFM where m_{t} is treated in $\overline{\mathrm{MS}}$ scheme
$\rightarrow$ EPJC 74 (2014) 3167

- first top physics result obtained with rigorous likelihood-based unfolding
- **significantly improved precision** compared to other methods

- $m_{\mathrm{t}}(m_{\mathrm{t}})$ extracted in each bin of $m_{\mathrm{t\bar{t}}}$ independently via χ^2 fit
- $m_{\mathrm{t}}(m_{\mathrm{t}})$ converted to $m_{\mathrm{t}}(\mu_k)$ using one-loop RGE solutions

result for $d\sigma_{t\bar{t}}/dm_{t\bar{t}}$ and extraction of $m_t(\mu)$

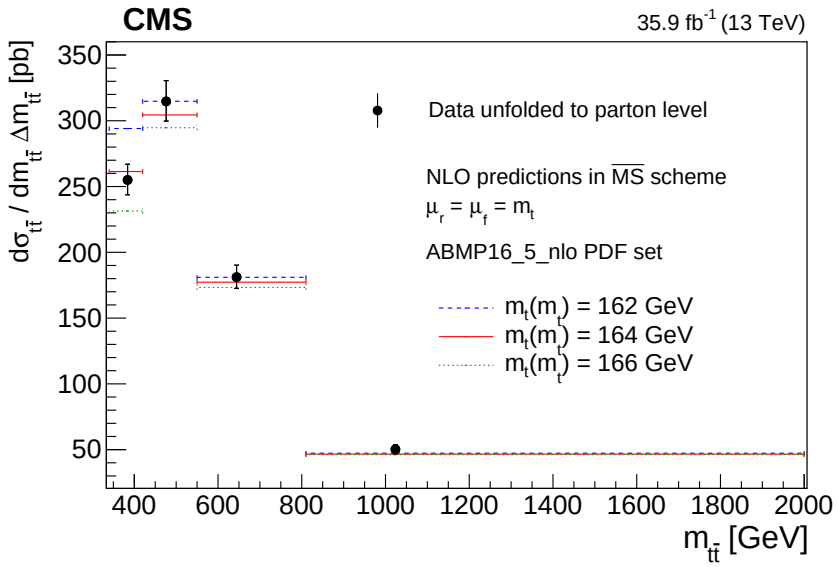

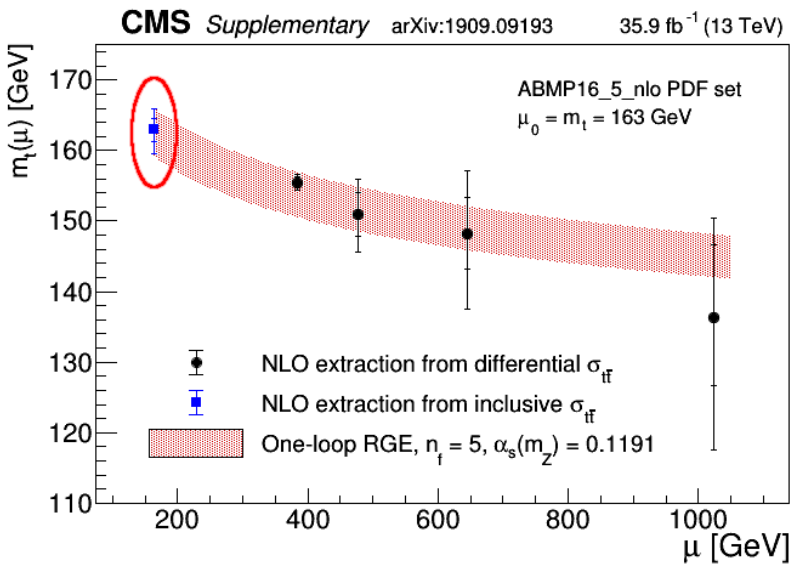

NLO predictions obtained with version of MCFM where m_t is treated in $\overline{\mathrm{MS}}$ scheme
→ EPJC 74 (2014) 3167

- first top physics result obtained with rigorous likelihood-based unfolding
- **significantly improved precision** compared to other methods

- $m_t(m_t)$ extracted in each bin of $m_{t\bar{t}}$ independently via χ^2 fit
- $m_t(m_t)$ converted to $m_t(\mu_k)$ using one-loop RGE solutions
- results compared to $m_t(m_t)$ obtained at NLO from inclusive $\sigma_{t\bar{t}}$

extraction of the running of m_t

running defined with respect to arbitrary reference scale $\mu_{ref} = \mu_2 = 476\,\text{GeV}$

$$\text{th:} \quad r(\mu) = m_t(\mu)/m_t(\mu_{ref})$$
$$\text{exp:} \quad r_k = m_t(\mu_k)/m_t(\mu_2)$$

1. th: depends solely on RGE
2. exp: benefits from cancellation of correlated uncertainties

- agreement with RGE prediction within 1.1 standard deviations
- no-running hypothesis excluded at $> 95\%$ confidence level

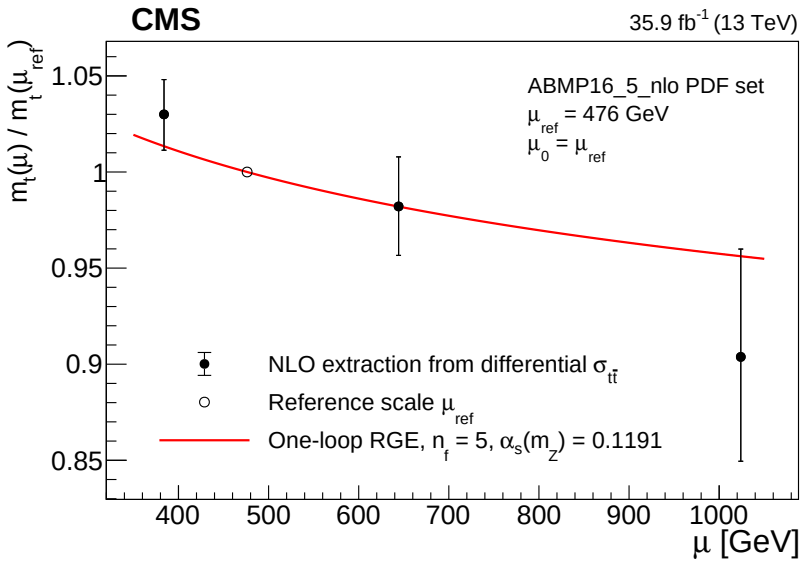

extraction of the running of m_t

running defined with respect to arbitrary reference scale $\mu_{\text{ref}} = \mu_2 = 476\,\text{GeV}$

$$\text{th:} \quad r(\mu) = m_t(\mu)/m_t(\mu_{\text{ref}})$$
$$\text{exp:} \quad r_k = m_t(\mu_k)/m_t(\mu_2)$$

1. th: depends solely on RGE
2. exp: benefits from cancellation of correlated uncertainties

- agreement with RGE prediction within 1.1 standard deviations
- no-running hypothesis excluded at $> 95\%$ confidence level
- compared to $m_t(m_t)/m_t(\mu_{\text{ref}})$ as determined from inclusive $\sigma_{t\bar{t}}$

$\rightarrow$ **running of a quark mass probed up to the TeV scale for the first time**

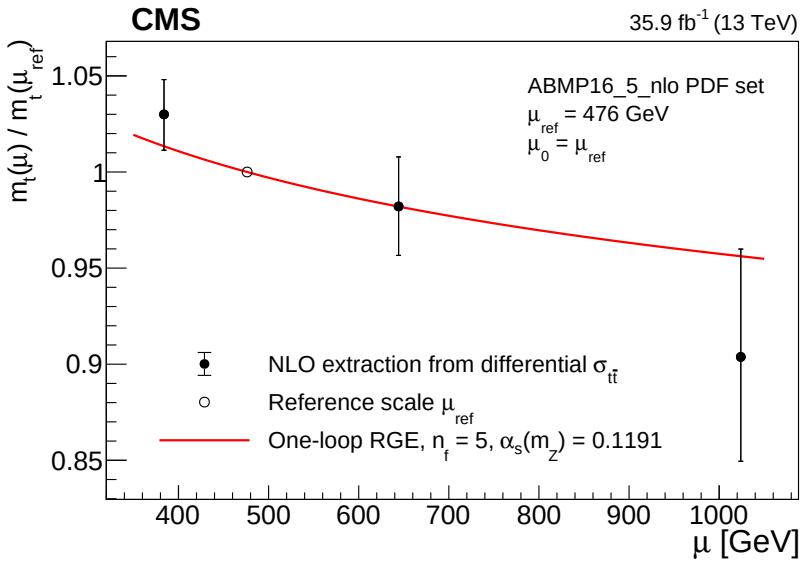

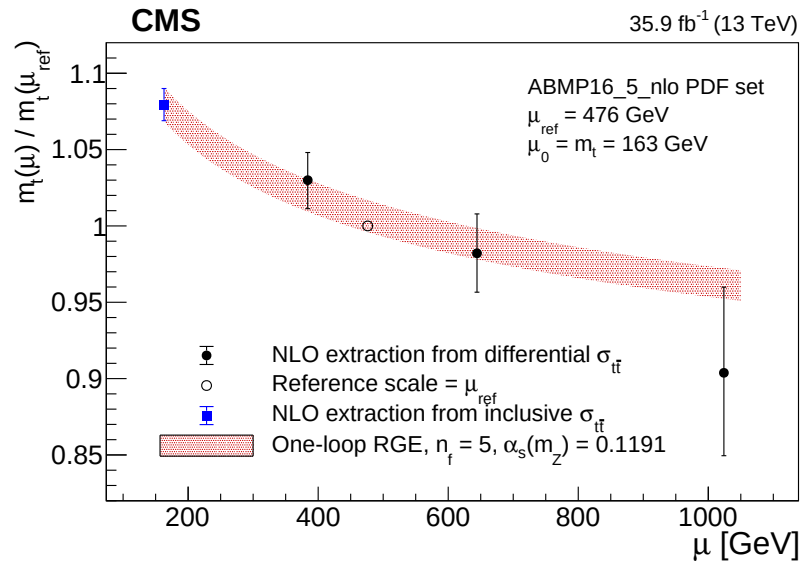

Measurement of the triple-differential $\mathrm{t\bar{t}}$ production cross section at $\sqrt{s} = 13\,\mathrm{TeV}$

and global QCD analysis with HERA DIS data: α_S, m_t, PDFs

motivation: taking a step back

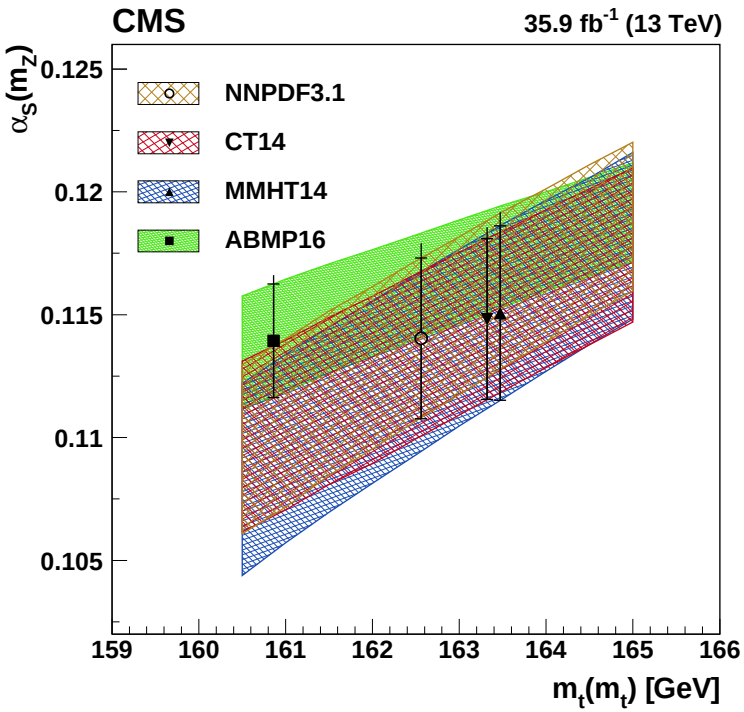

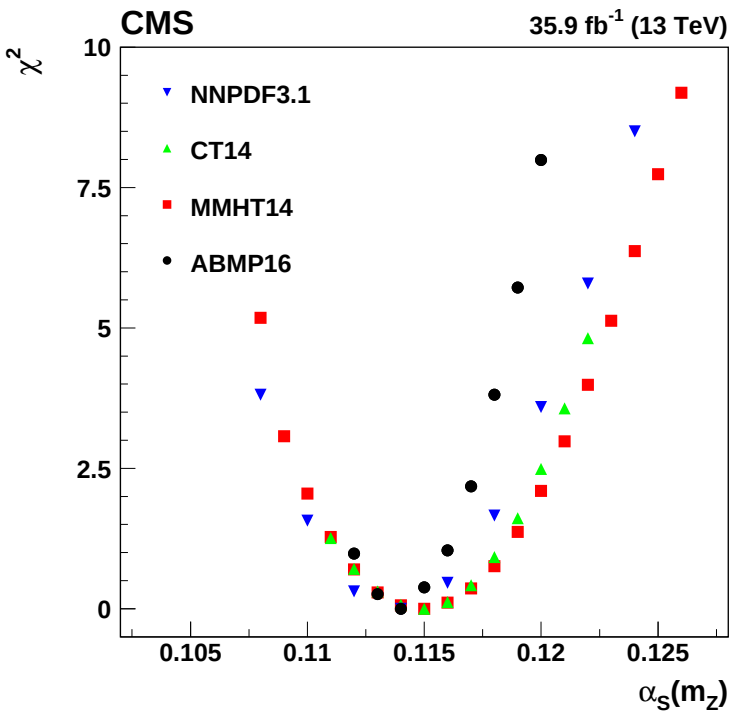

inclusive cross section

- strong correlation between m_{t} and α_{S}
- modest dependence of α_{S} on PDFs

solution: simultaneous determination of QCD parameters and PDFs

$\rightarrow$ triple-differential $\mathrm{t\bar{t}}$ cross section

normalized triple-differential $\mathrm{t\bar{t}}$ cross section

- events in all di-leptonic channels ($\mathrm{e^{\mp}\mu^{\pm}}$, $\mathrm{e^{+}e^{-}}$, $\mu^{+}\mu^{-}$)
- more stringent event selection wrt inclusive/running analyses $\rightarrow$ higher purity
- backgrounds are subtracted before χ^2-based regularized unfolding

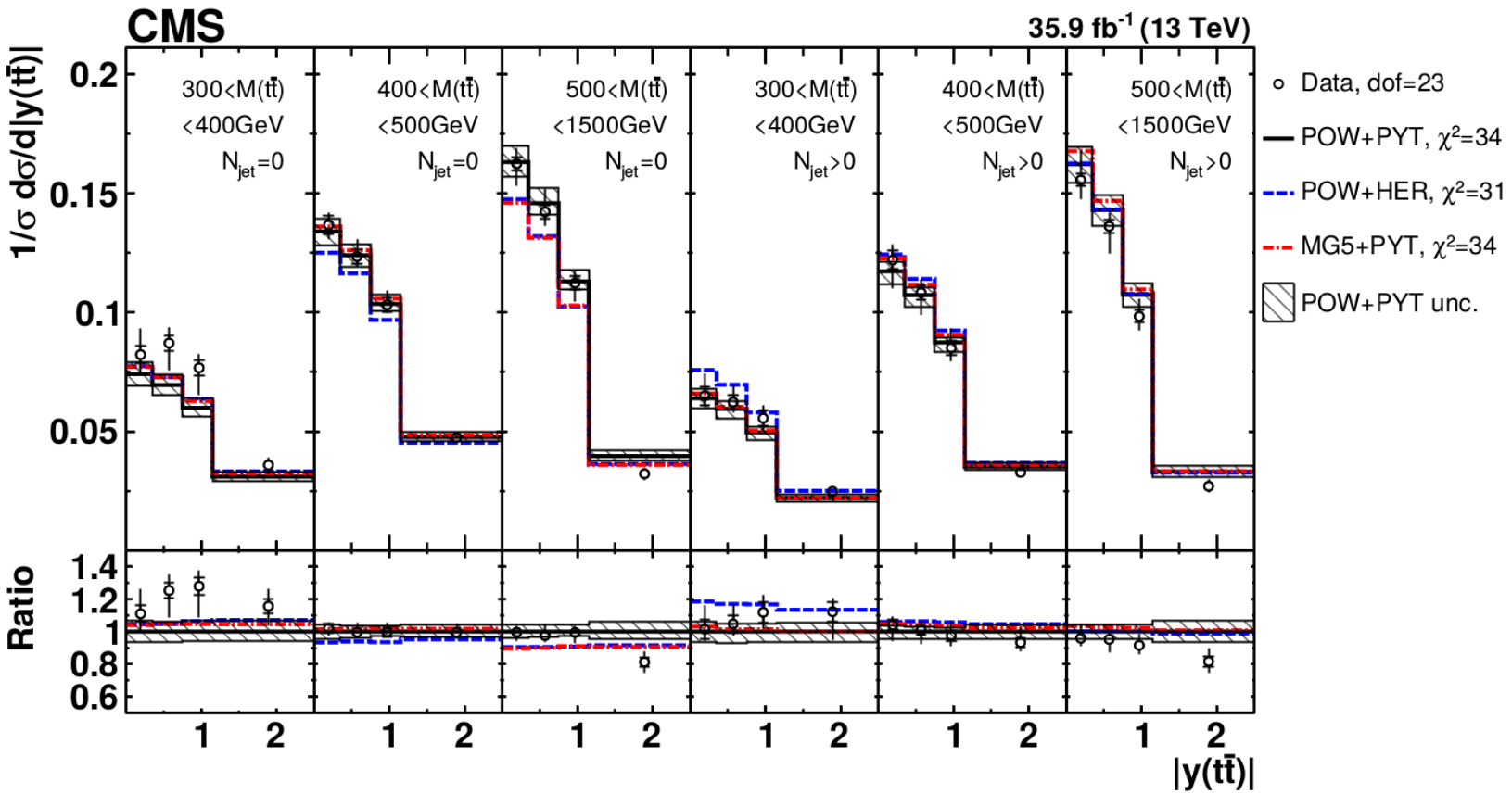

normalized triple-differential $\mathrm{t\bar{t}}$ cross section

- measured as a function of $|\boldsymbol{y(\mathrm{t\bar{t}})}|$, N_{jet}, $M(\mathrm{t\bar{t}})$

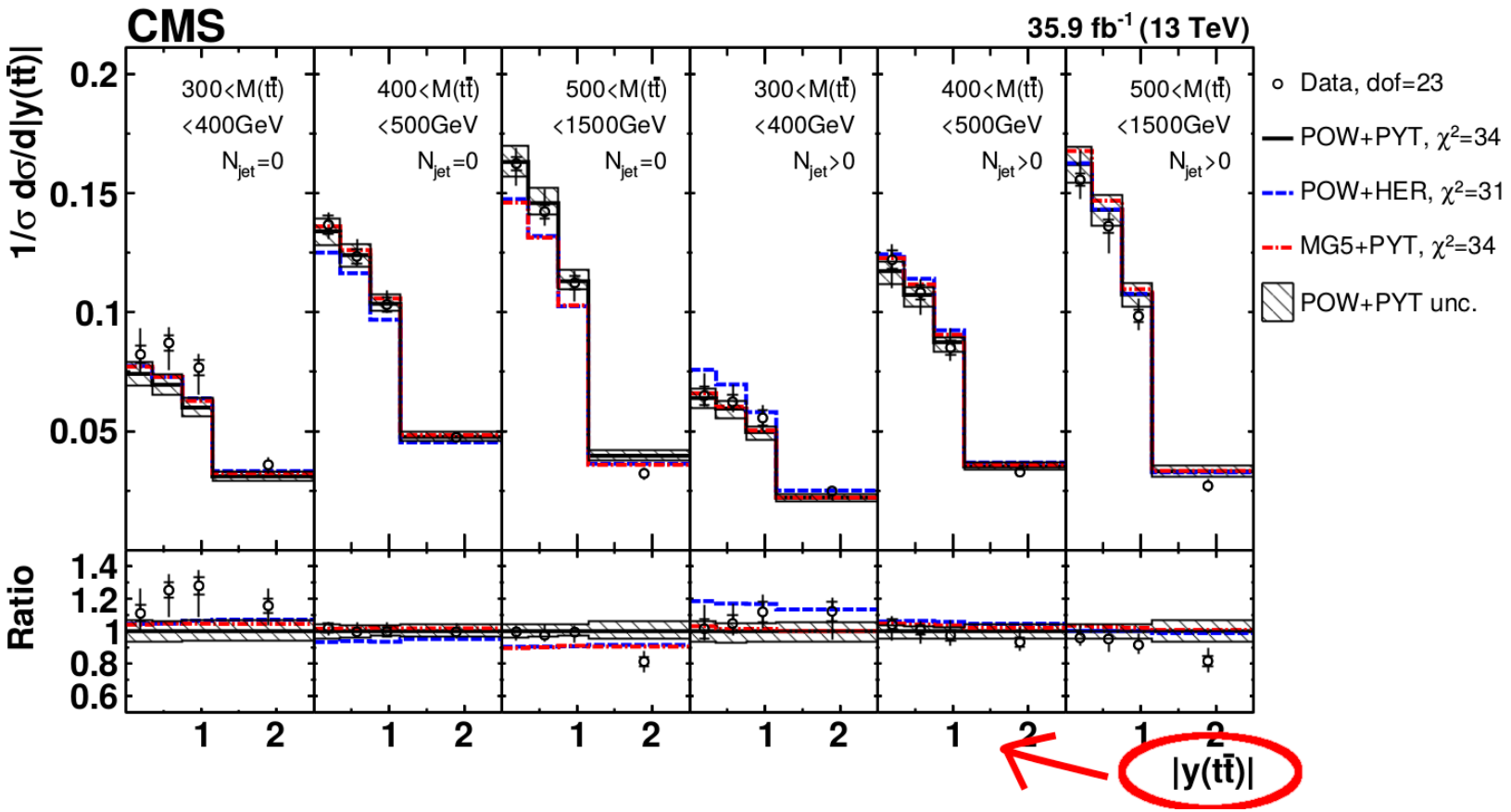

normalized triple-differential $\mathrm{t\bar{t}}$ cross section

- measured as a function of $|y(\mathrm{t\bar{t}})|$, $\boldsymbol{N}_{\mathrm{jet}}$, $M(\mathrm{t\bar{t}})$

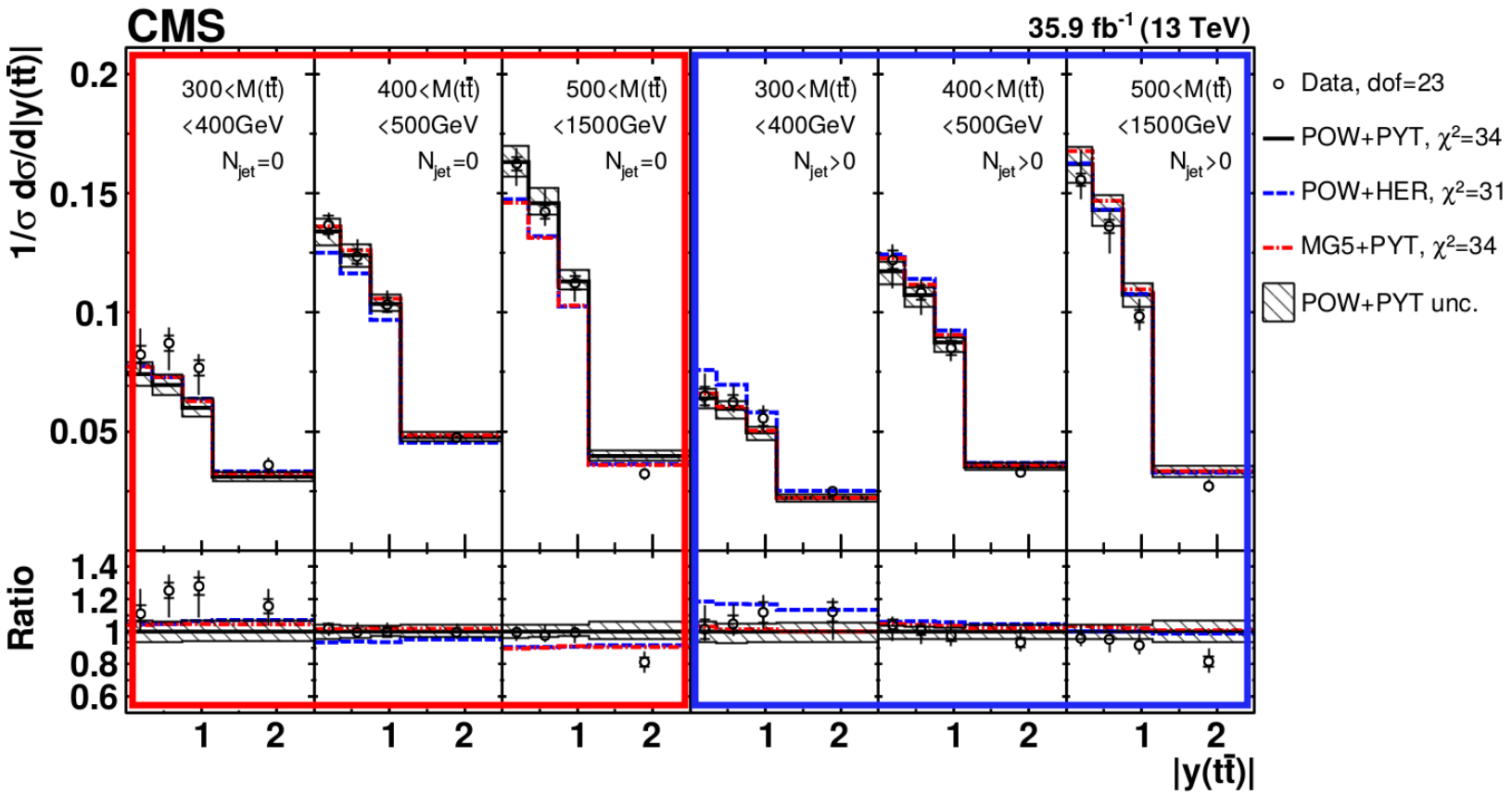

normalized triple-differential $\mathrm{t\bar{t}}$ cross section

- measured as a function of $|y(\mathrm{t\bar{t}})|$, N_{jet}, $\boldsymbol{M(\mathrm{t\bar{t}})}$

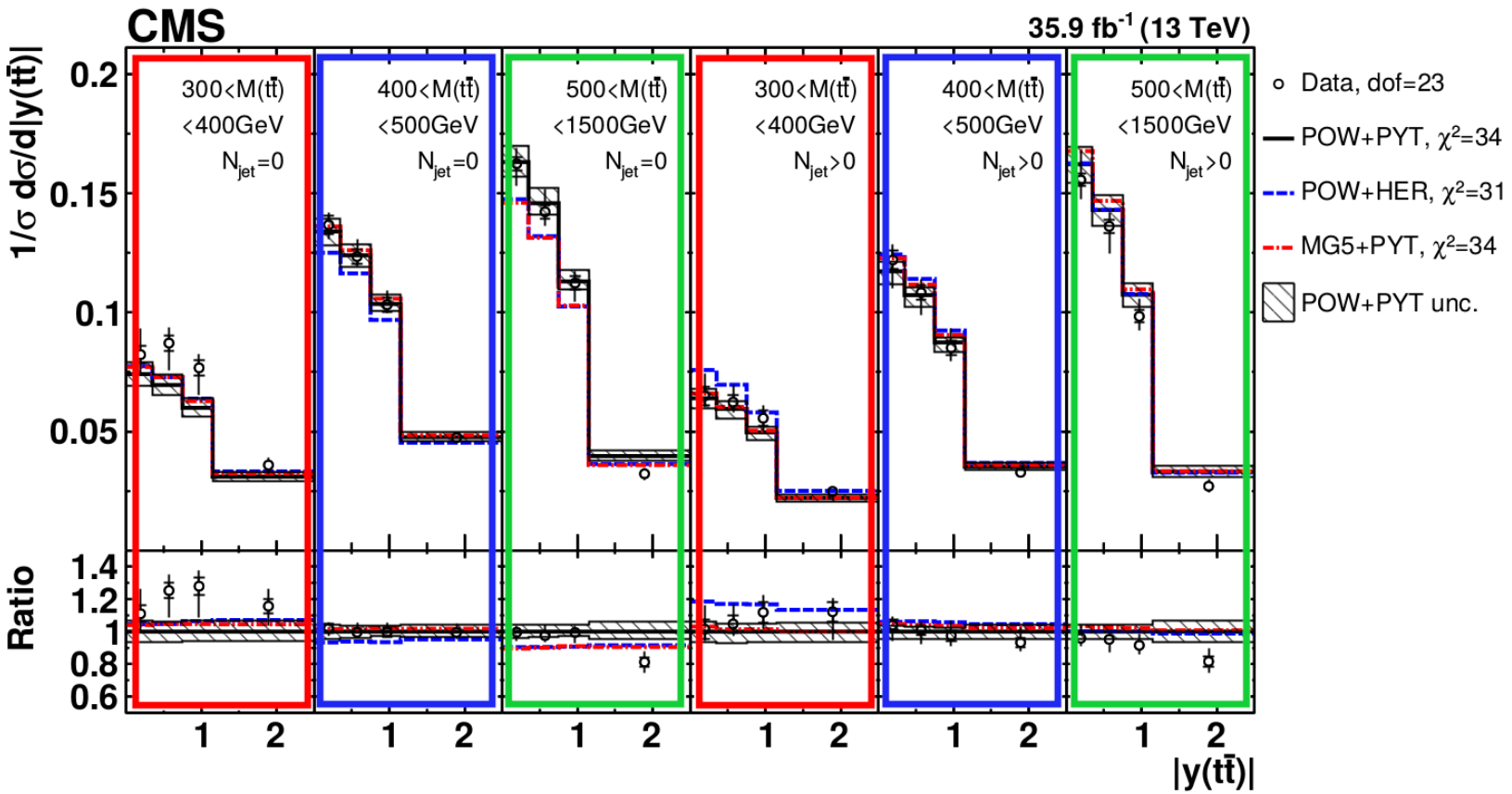

normalized triple-differential $\mathrm{t\bar{t}}$ cross section

- measured as a function of $|y(\mathrm{t\bar{t}})|$, N_{jet}, $M(\mathrm{t\bar{t}})$
- particle-level result compared to different event generators

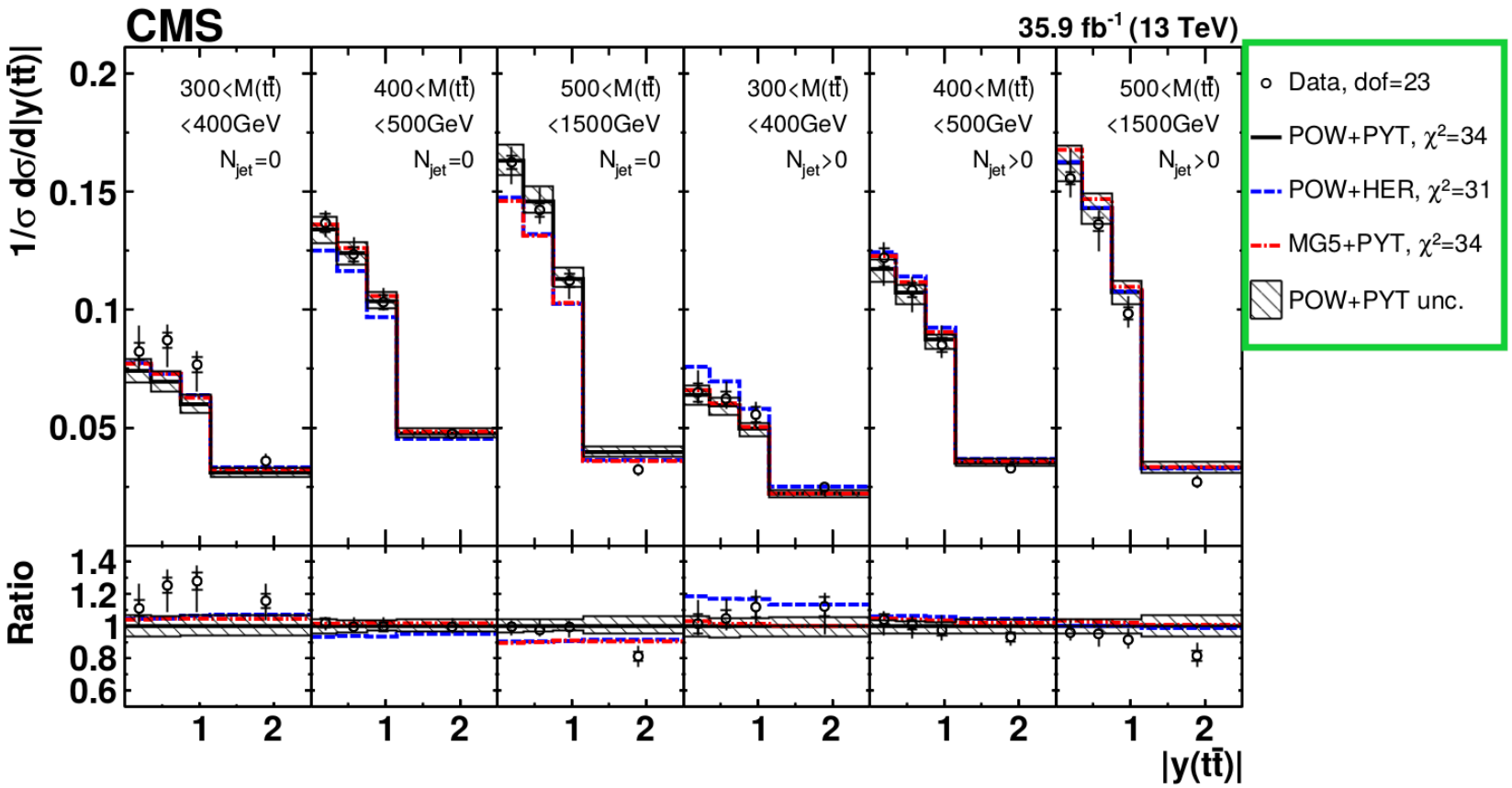

choice of variables

1. N_{jet} strongly dependent on value of α_{S}

choice of variables

1. N_{jet} strongly dependent on value of α_{S}
2. threshold of $M(\text{t}\bar{\text{t}})$ sensitive to value of m_{t}

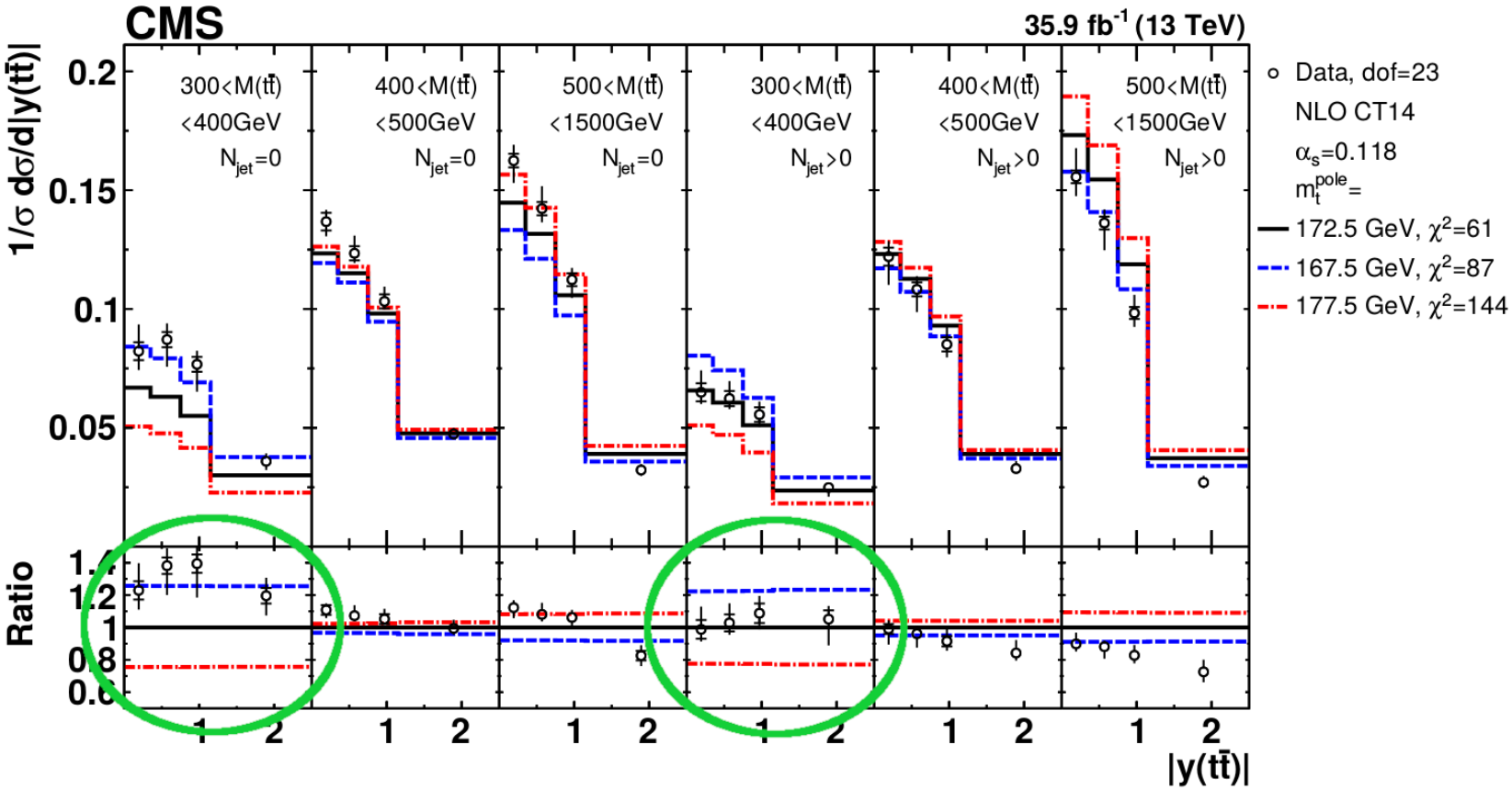

choice of variables

1. N_{jet} strongly dependent on value of α_{S}
2. threshold of $M(\text{t}\bar{\text{t}})$ sensitive to value of m_{t}
3. at LO, $x_B = \frac{M(\text{t}\bar{\text{t}})}{\sqrt{s}e^{\pm y(\text{t}\bar{\text{t}})}} \rightarrow$ (gluon) PDFs

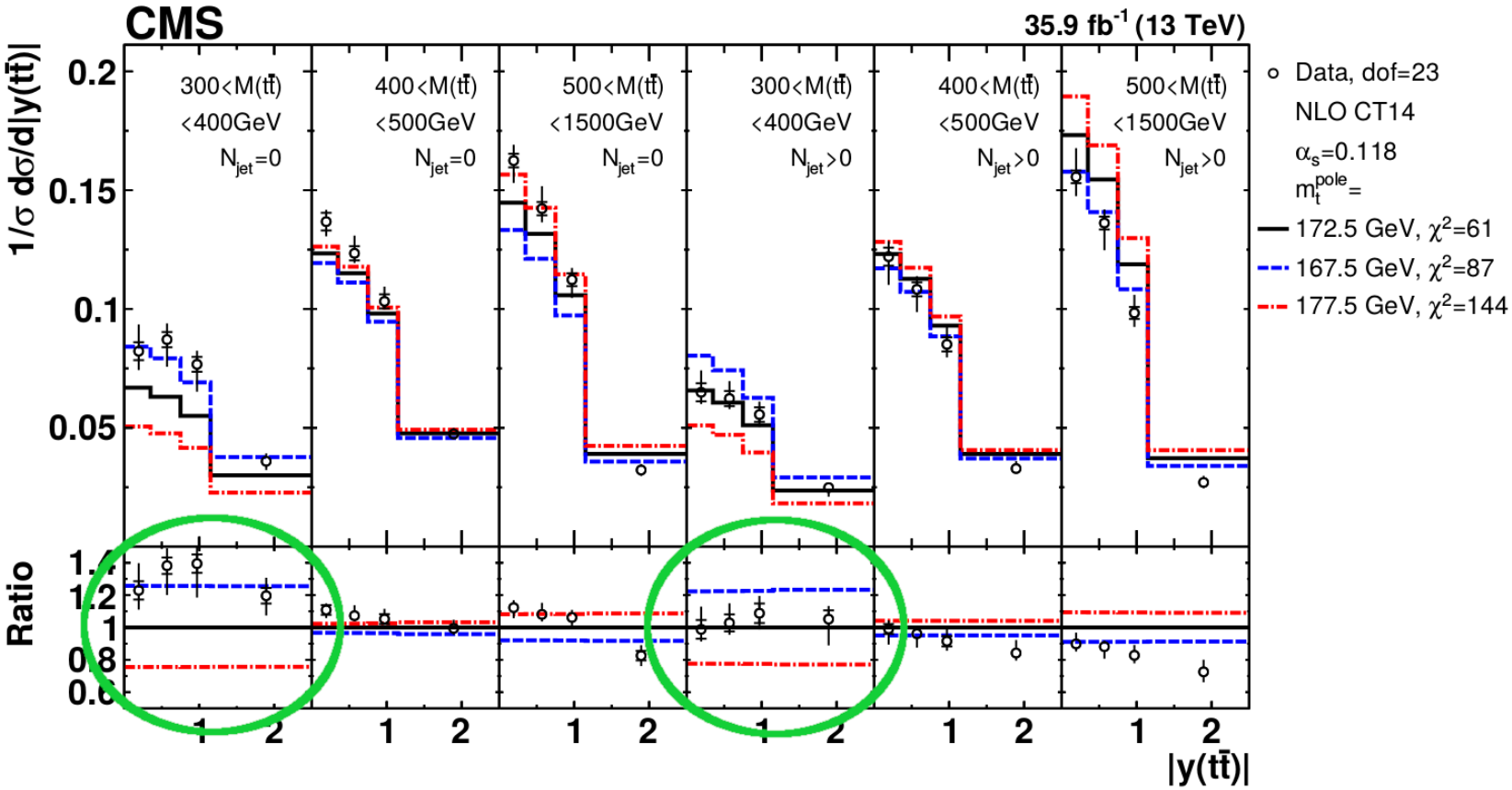

choice of variables

1. N_{jet} strongly dependent on value of α_S
2. threshold of $M(t\bar{t})$ sensitive to value of m_t
3. at LO, $x_B = \frac{M(t\bar{t})}{\sqrt{s}e^{\pm y(t\bar{t})}} \rightarrow$ (gluon) PDFs

caveat: shape of threshold region affected by choice of m_t in kinematic reconstruction

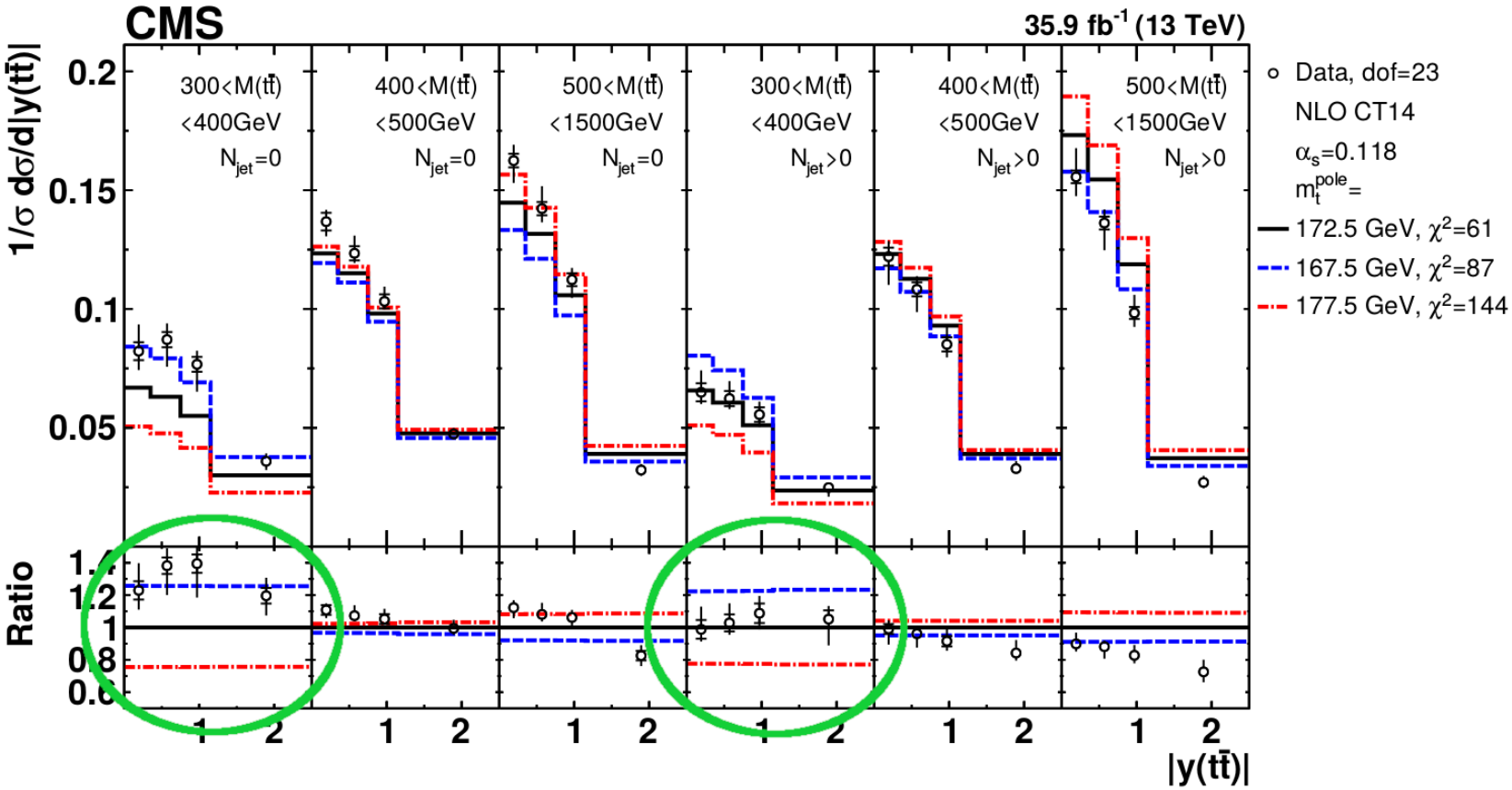

loose kinematic reconstruction

new kinematic reconstruction method developed for this analysis

full kinematic reconstruction

- separate reconstruction of t and $\bar{\mathrm{t}}$
- m_{t}, m_{W} constraint

$\rightarrow$ strong dependence on choice of m_{t}

however, chosen variables only depend on kinematic of $\mathrm{t}\bar{\mathrm{t}}$ system

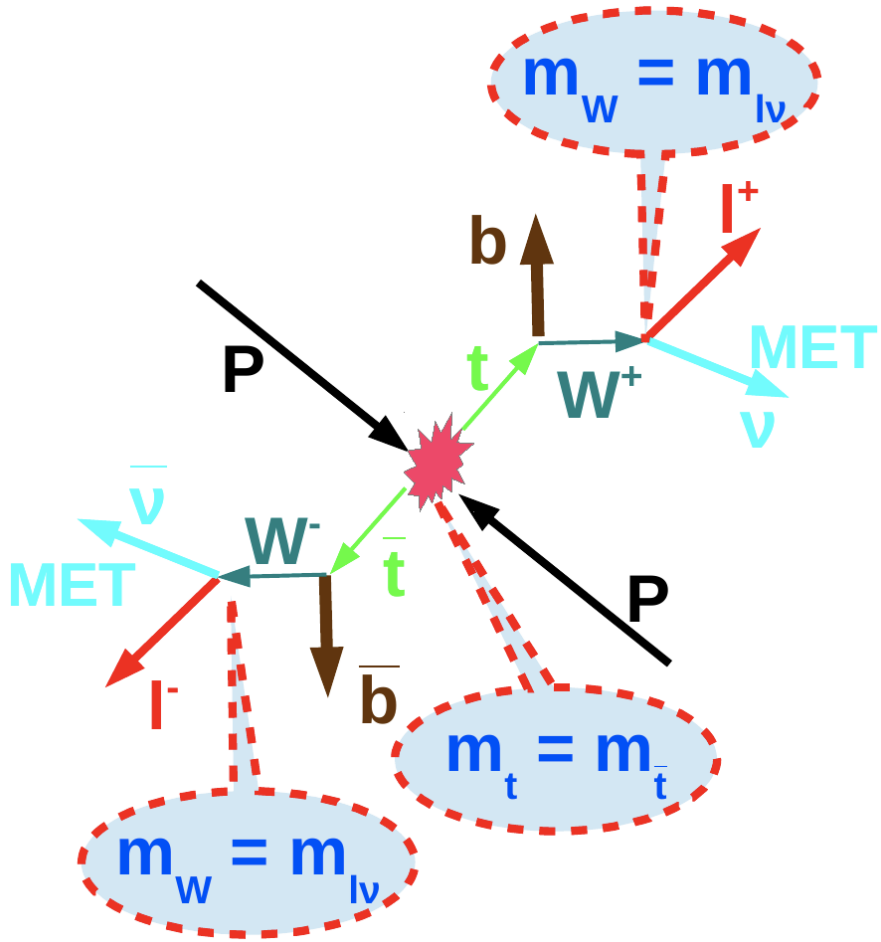

loose kinematic reconstruction

new kinematic reconstruction method developed for this analysis

full kinematic reconstruction

- separate reconstruction of t and $\bar{\mathrm{t}}$
- m_{t}, m_{W} constraint

$\rightarrow$ strong dependence on choice of m_{t}

however, chosen variables only depend on kinematic of $\mathrm{t}\bar{\mathrm{t}}$ system

loose kinematic reconstruction

- reconstruction of $\mathrm{t}\bar{\mathrm{t}}$ system
- m_{W} constraint only

$\rightarrow$ negligible dependence on m_{t}
$\rightarrow$ similar performance as full kin. reco.

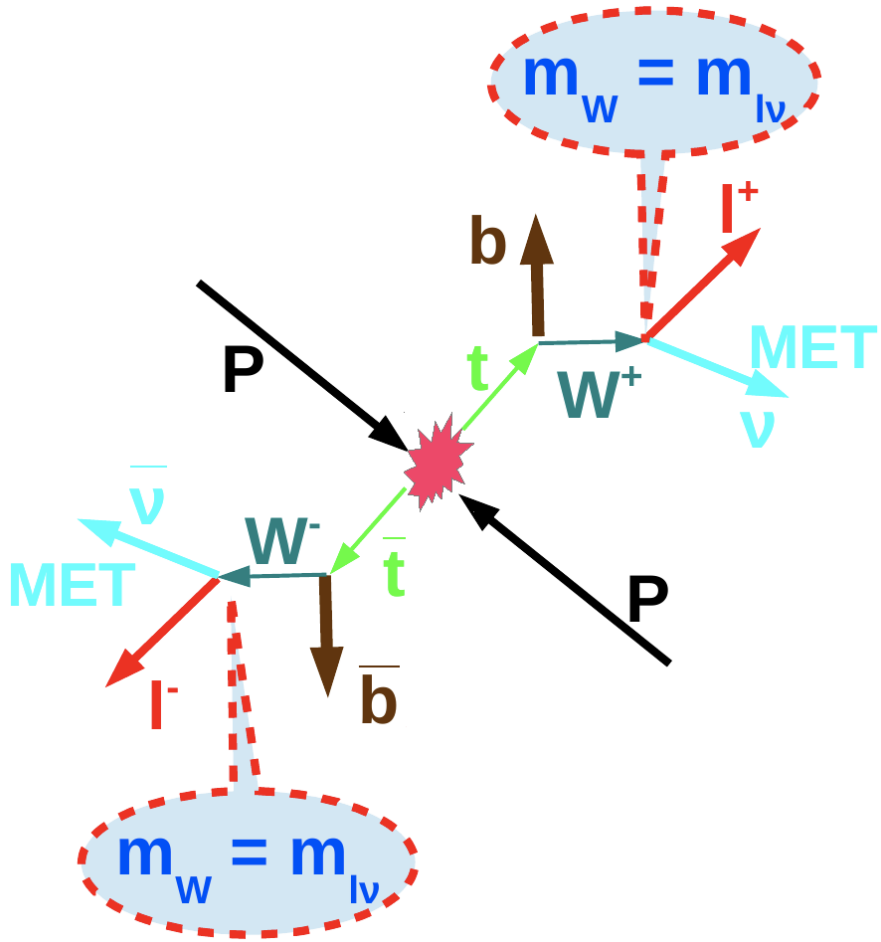

comparison to NLO predictions with external PDFs

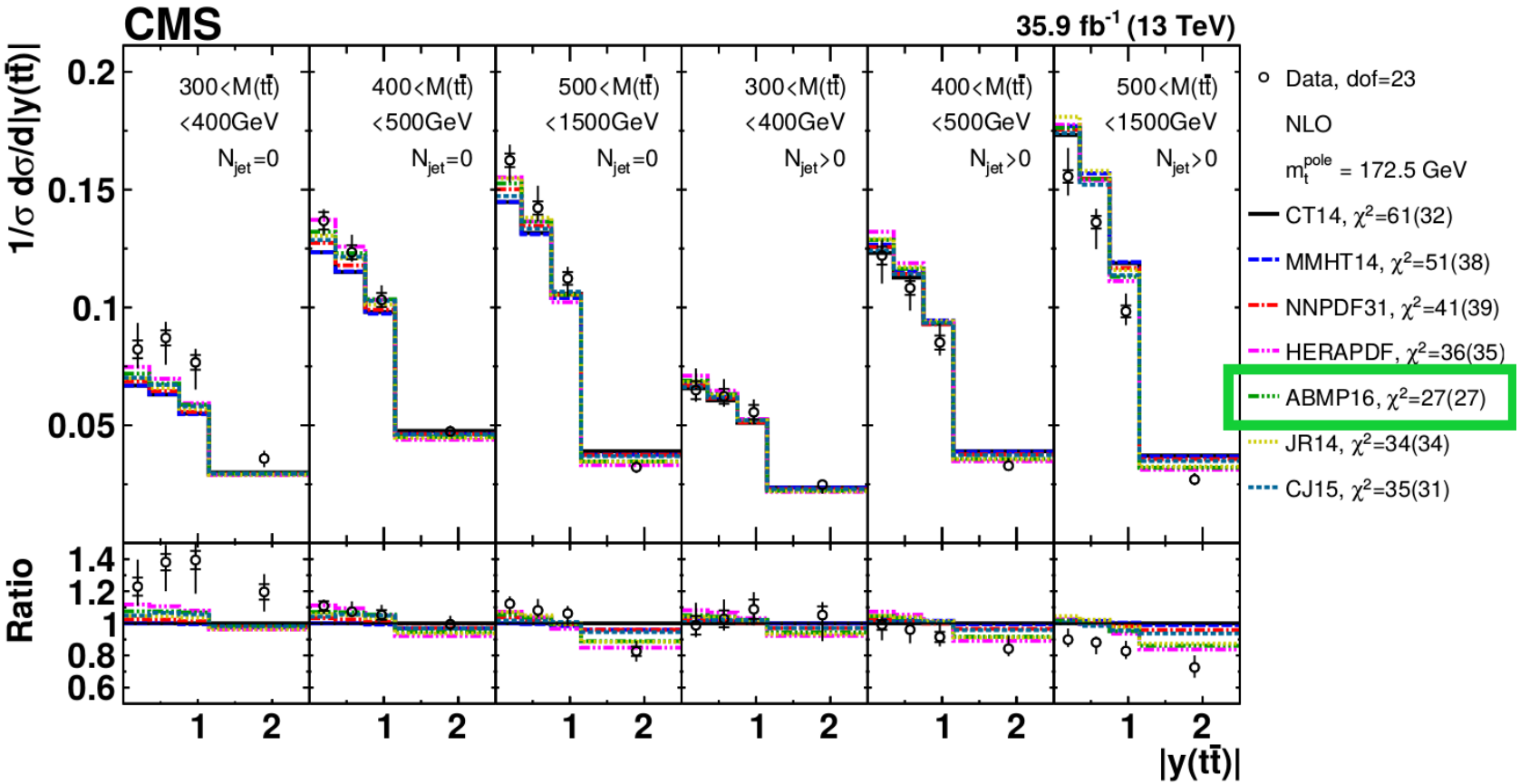

trends observed in all cases $\Rightarrow$ $t\bar{t}$ data can bring significant improvements

NB: values of α_S, m_t often assumed in PDFs $\Rightarrow$ important correlations neglected

global QCD analysis at NLO

- simultaneous determination of $\alpha_S(m_Z)$, m_t^{pole}, proton PDFs
- fit to HERA + CMS $t\bar{t}$ data

$t\bar{t}$ data

- mainly sensitive to gluon PDF
- sensitive to quark PDFs at large $M(t\bar{t})$

DIS data

- precise determination of quark PDFs
- gluon PDF mainly from scaling violation $\rightarrow$ significant improvement expected with $t\bar{t}$ data

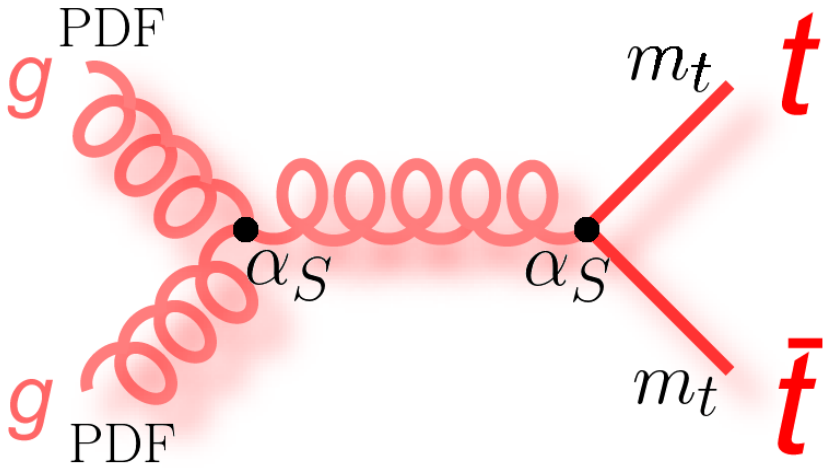

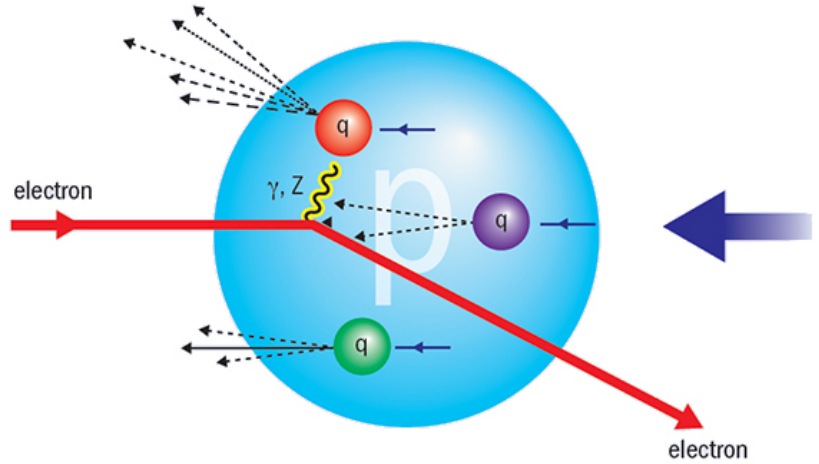

results for $\alpha_S(m_Z)$ and m_t^{pole}

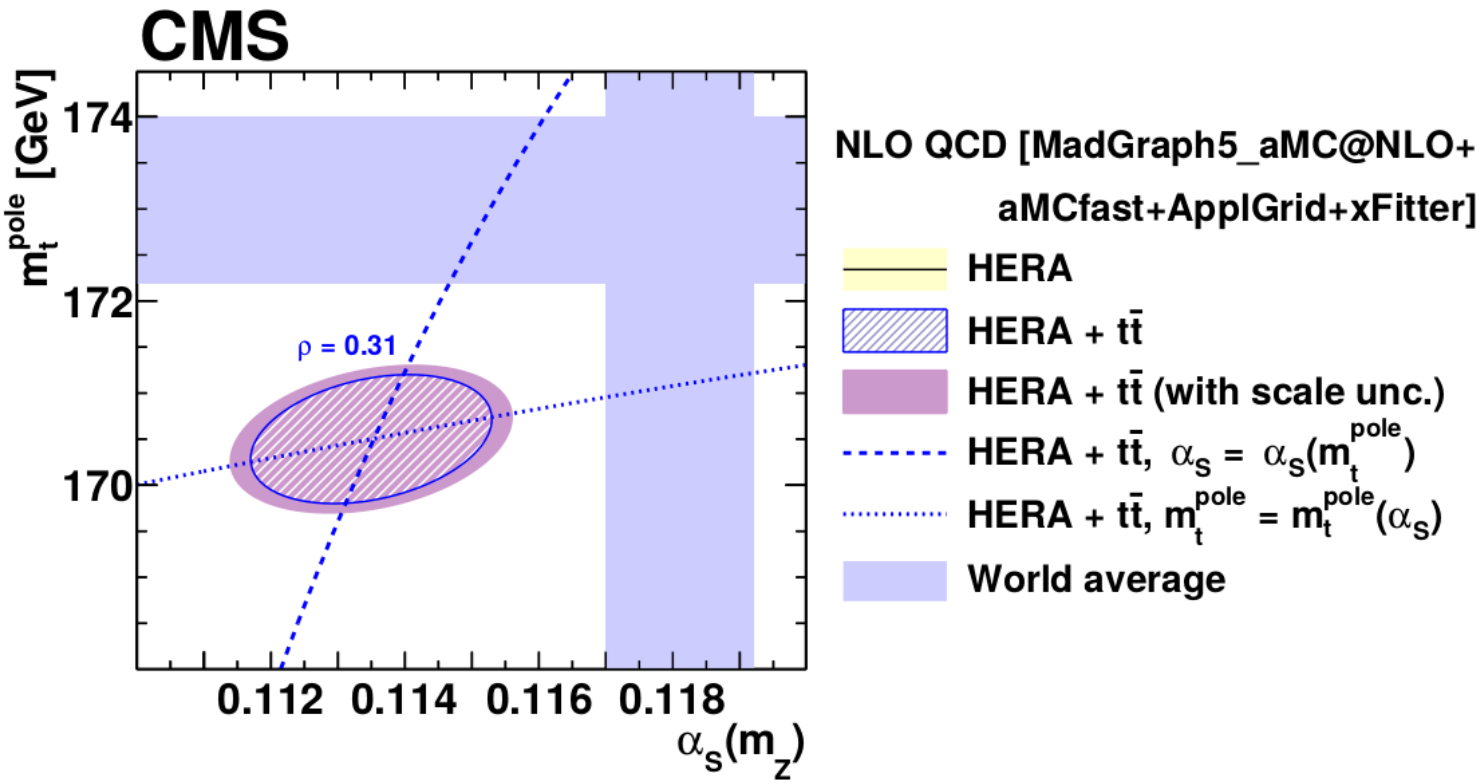

- results consistent with those from inclusive $\sigma_{t\bar{t}}$ (ABMP16)
- $m_t^{pole} = 170.5 \pm 0.8\,\text{GeV} \Rightarrow$ **most precise determination to date**

caveats

- results are obtained at NLO
- missing threshold corrections can have large effect on m_t^{pole} (order 1 GeV)

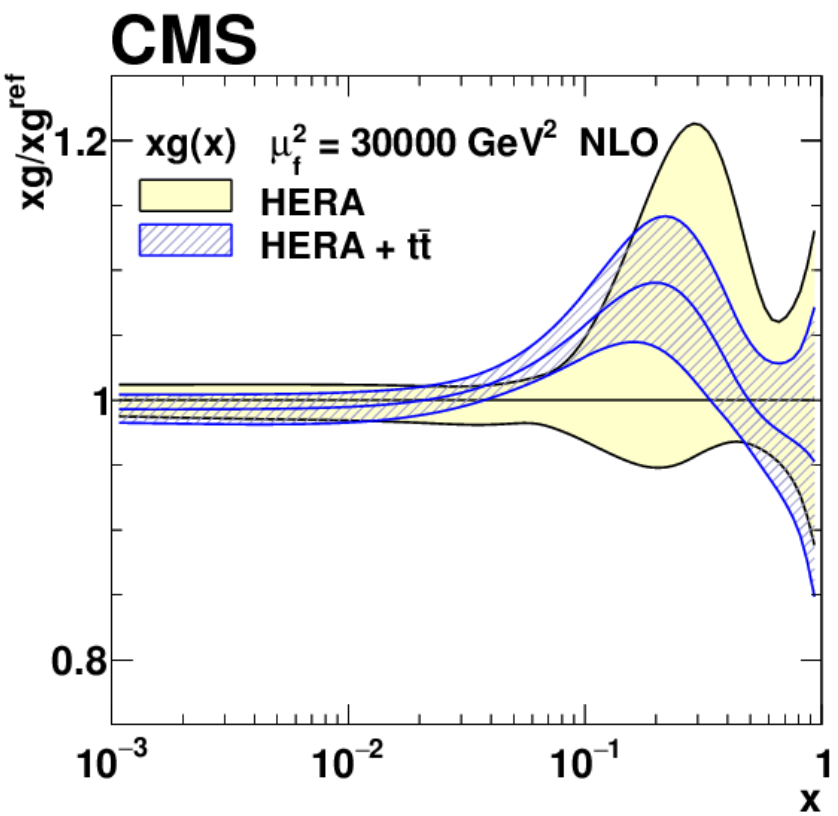

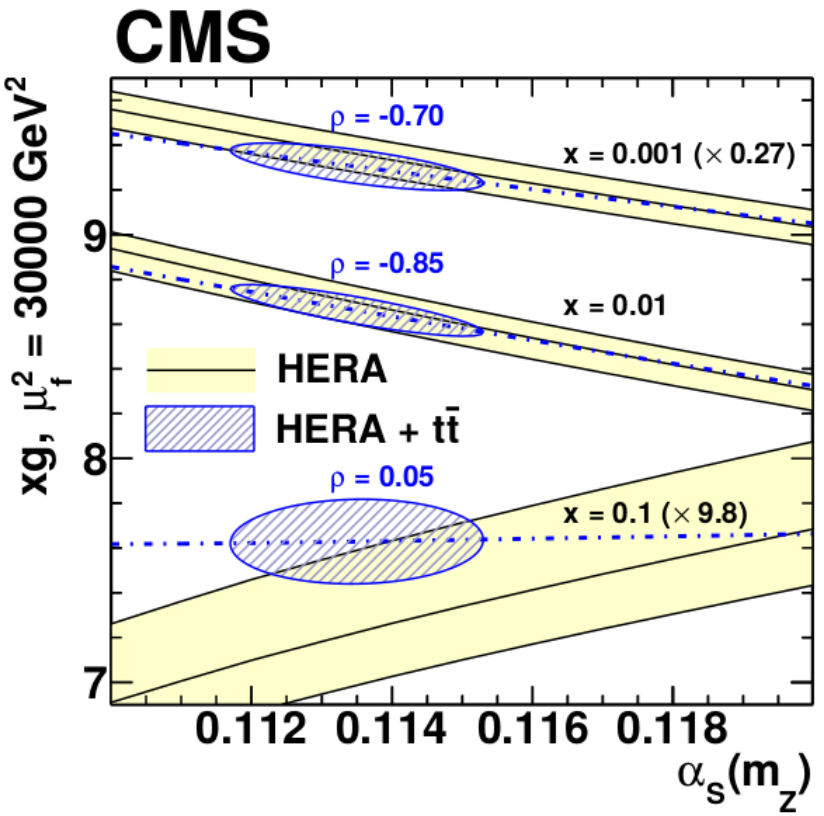

- uncertainty on gluon PDF significantly reduced in sensitive range ($x_B \simeq 0.1$)
- correlation between α_S and gluon PDF significantly mitigated

data/theory agreement after the fit

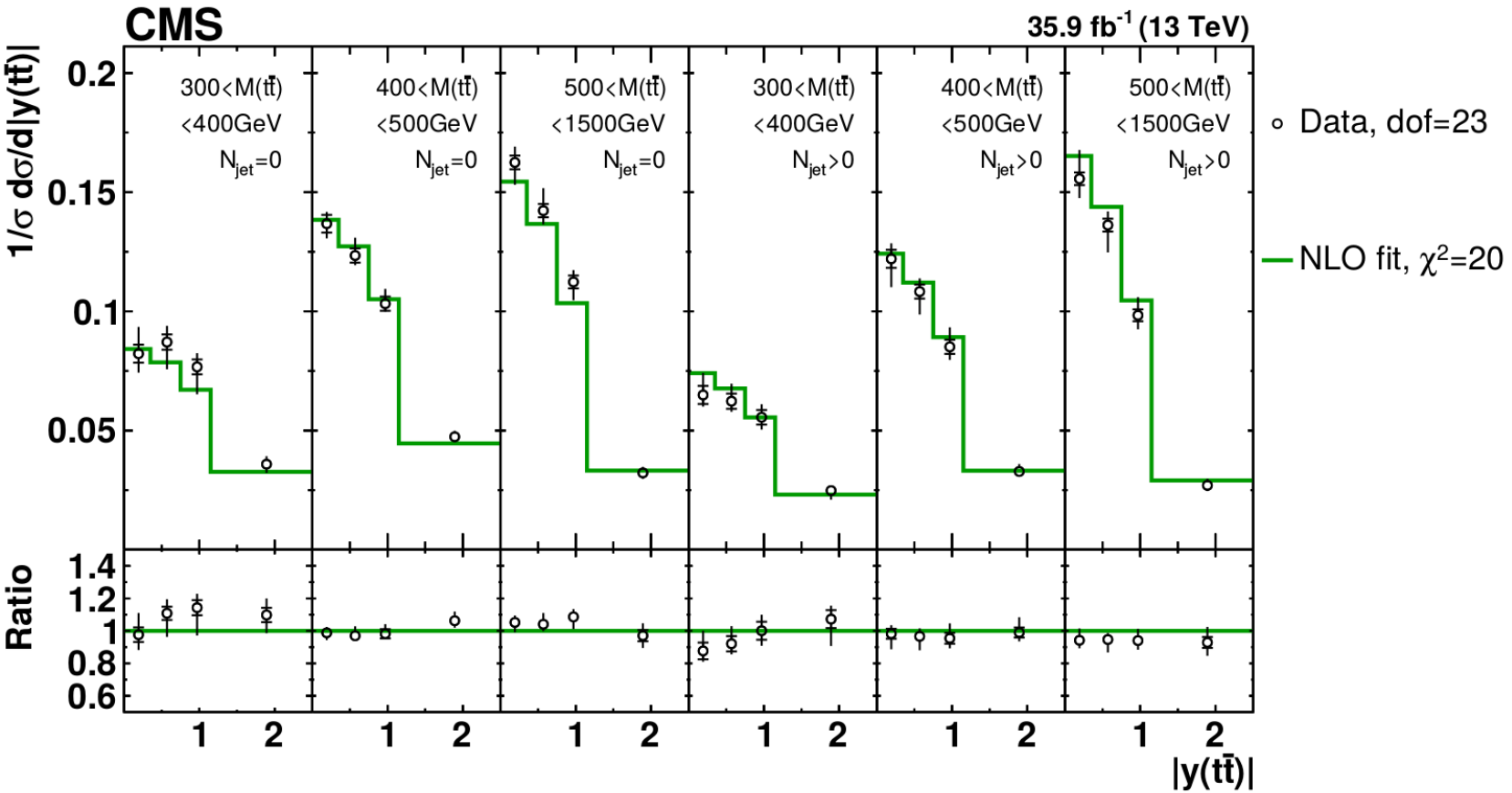

- remarkable agreement after the fit
  → improved wrt external PDFs
- benefits from proper account for correlation between QCD parameters

most recent CMS measurements of $\mathrm{t\bar{t}}$ data used to probe pQCD

- simultaneous measurement of $\sigma_{\mathrm{t\bar{t}}}$ and $m_{\mathrm{t}}^{\mathrm{MC}}$
- determination of α_{S} and m_{t} at NNLO

$\rightarrow$ EPJC 79 (2019) 368

1. most precise NNLO measurement of α_{S} at hadron collider
2. first consistent determination of $m_{\mathrm{t}}(m_{\mathrm{t}}) \rightarrow 1.2\%$ precision

possible improvements

- luminosity and lepton ID uncertainties
- threshold resummation in $\overline{\mathrm{MS}}$ scheme

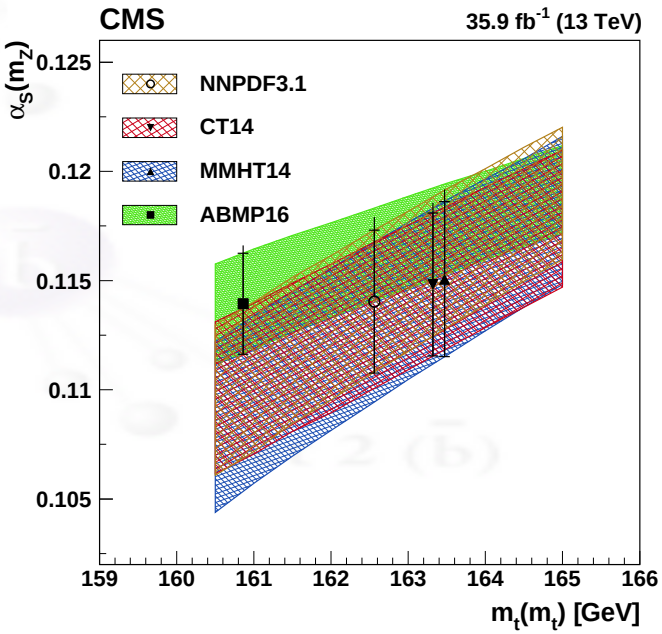

- **first measurement of running of the top quark mass**
  $\rightarrow$ PLB 803 (2020) 135263
- investigated up to the TeV scale

possible improvements

- same as for inclusive analysis
- higher order calculations in $\overline{\text{MS}}$ scheme
- dynamic scales in calculation

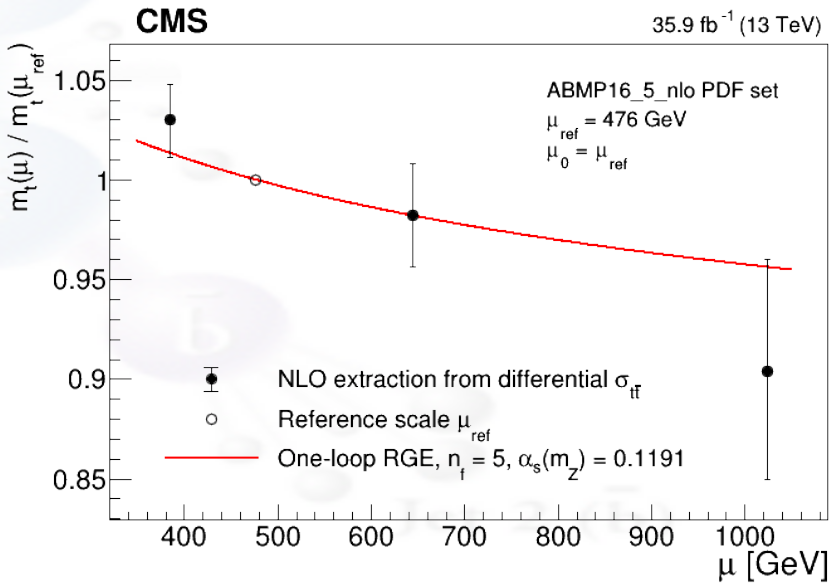

- global QCD analysis of CMS triple-differential $\mathrm{t\bar{t}}$ cross section and HERA data → arXiv:1904.05237 (accepted by EPJC)
- simultaneous determination of α_S, m_t, PDF

→ among most precise determination of QCD parameters are obtained
→ method takes all correlations into account

possible improvements

- theory predictions beyond NLO
- will benefit from additional statistics collected during Run2 (x4) and upcoming Run3 (x10)

→ better understanding of $\mathrm{t\bar{t}}$ production near threshold needed

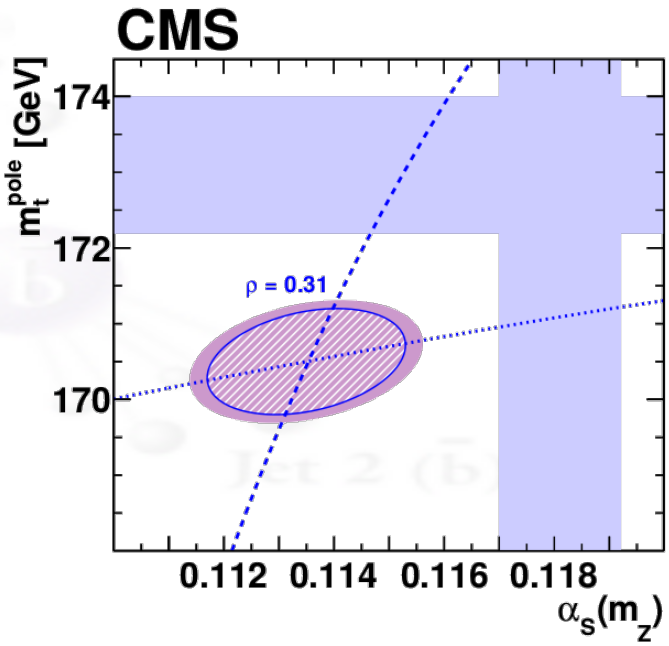

Thank you for your attention!

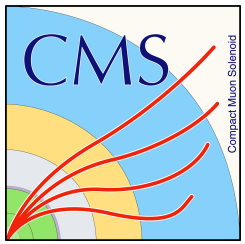

summary plot: $\sigma_{t\bar{t}}$ vs $\sqrt{s}$

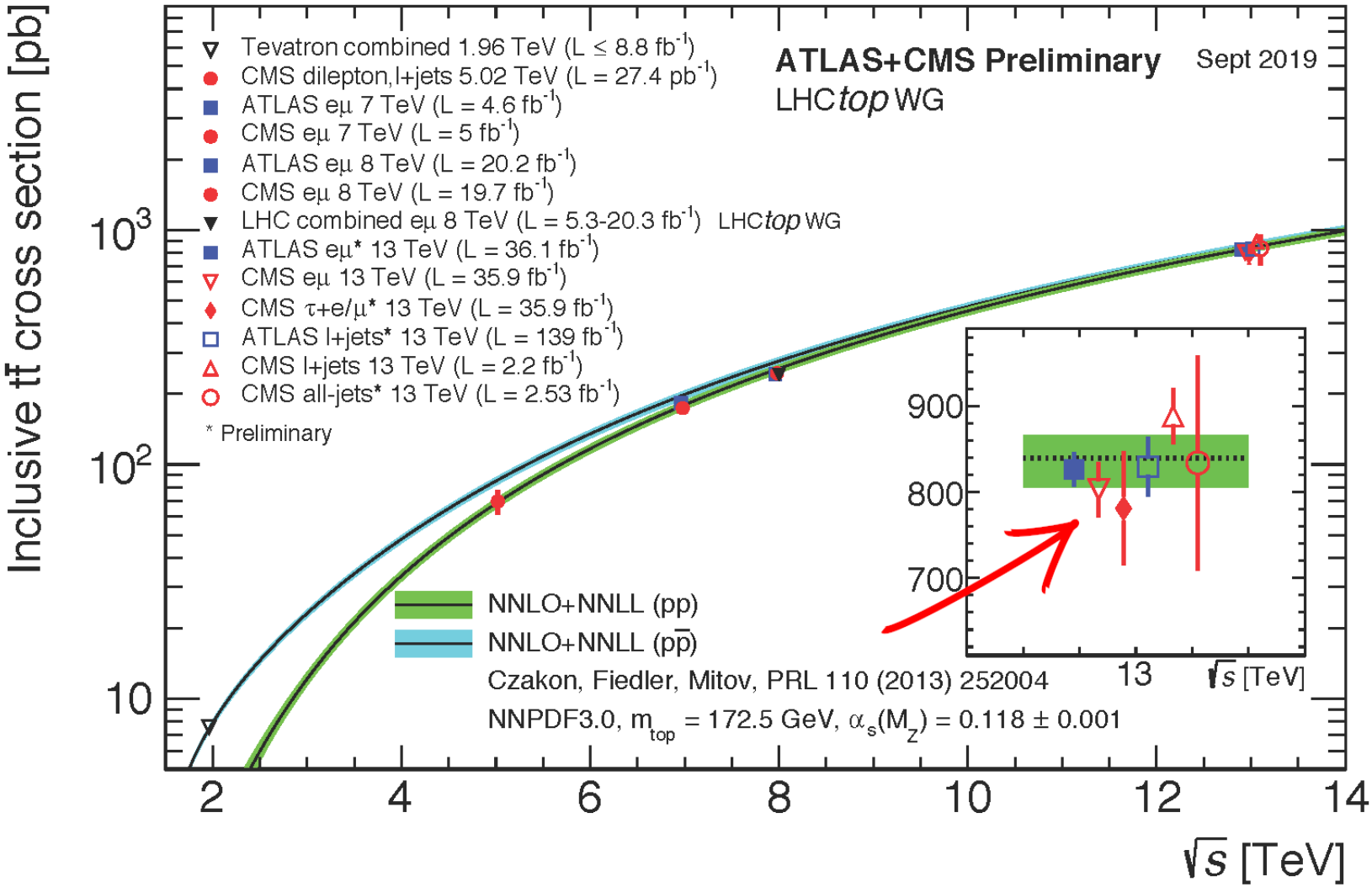

summary plot: $\sigma_{t\bar{t}}$ at 13 TeV

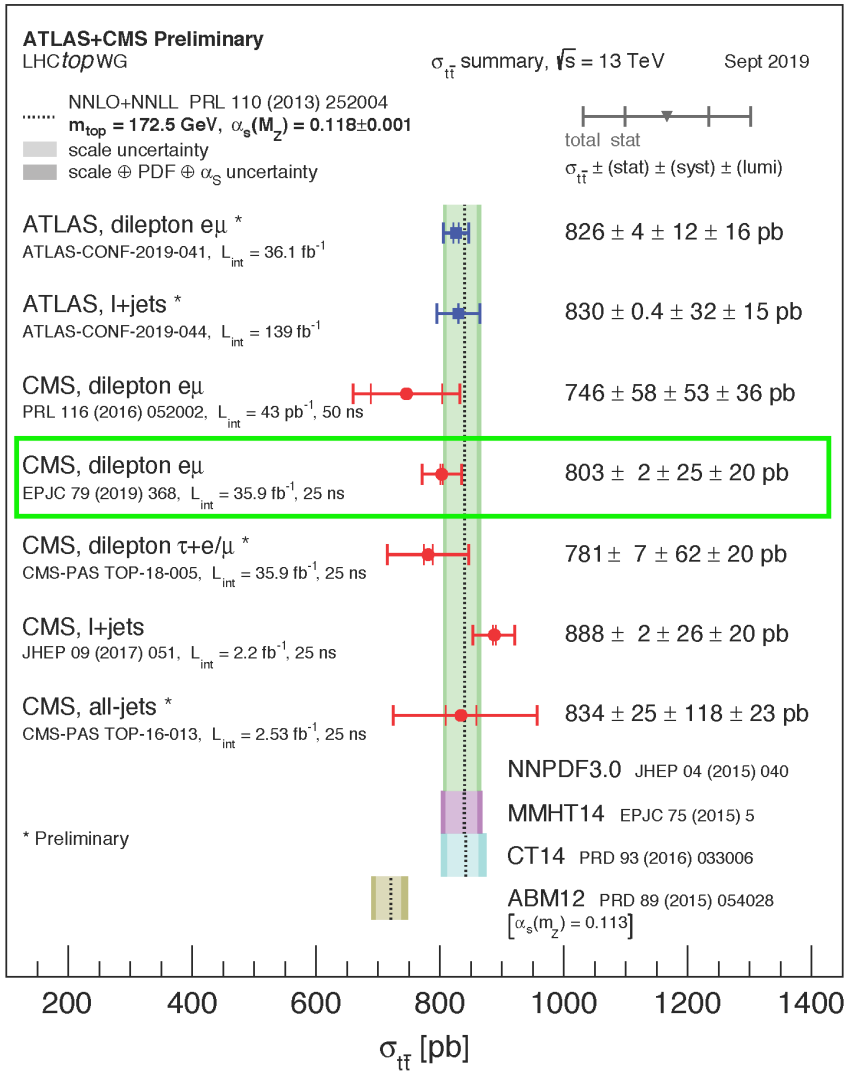

summary plot: m_t^{MC}

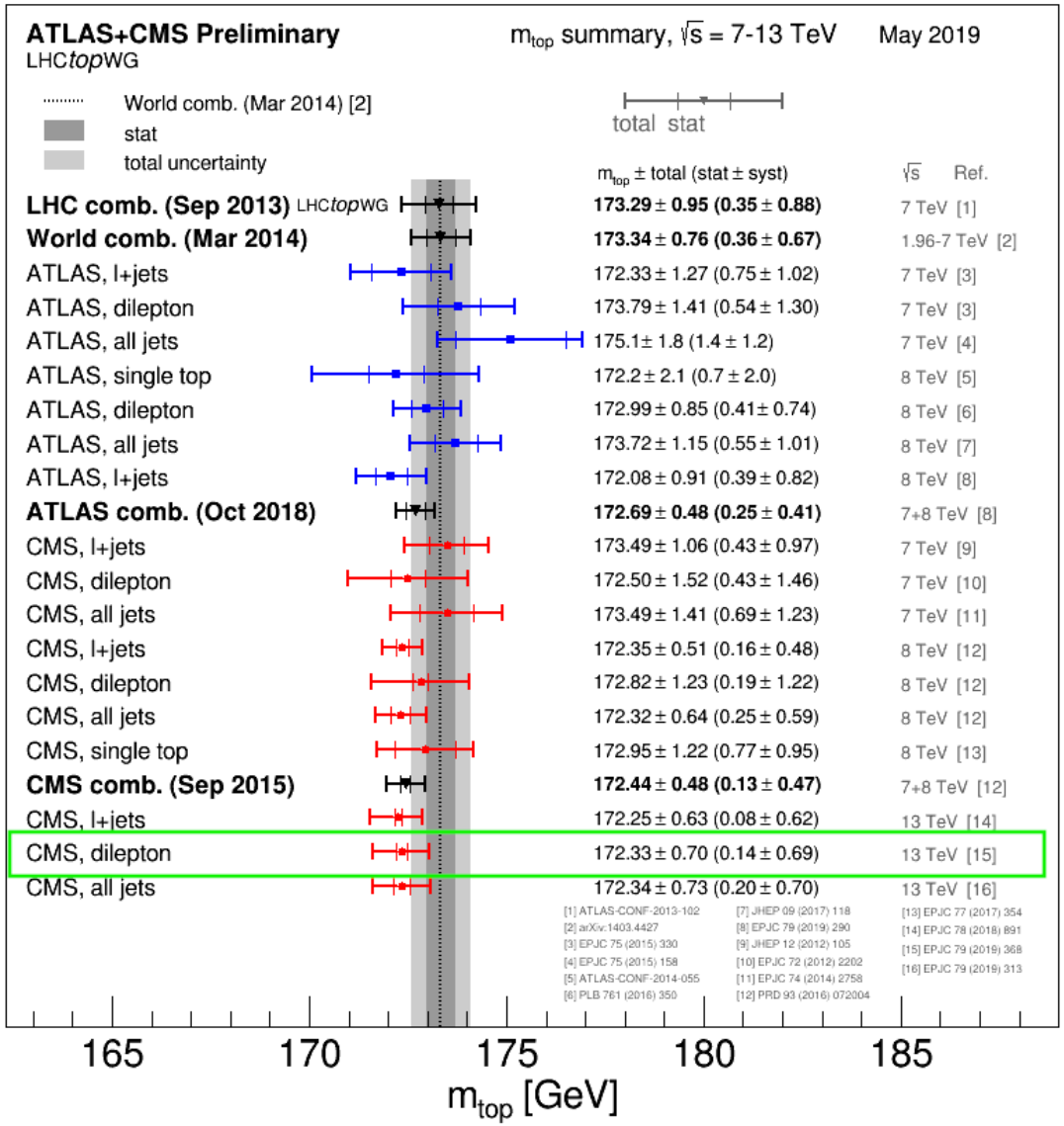

summary plot: m_t^{pole}

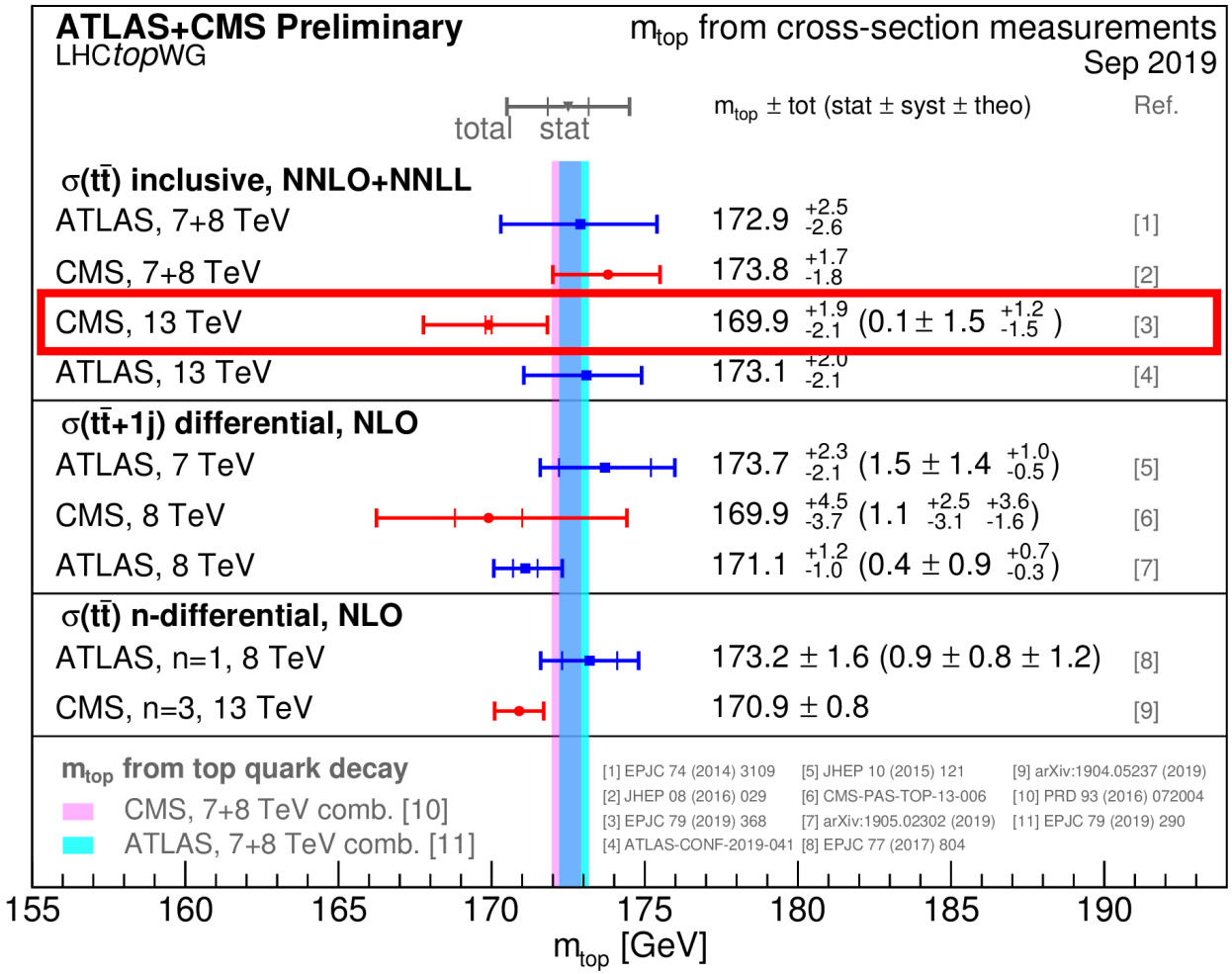

summary plot: $\alpha_S(m_Z)$

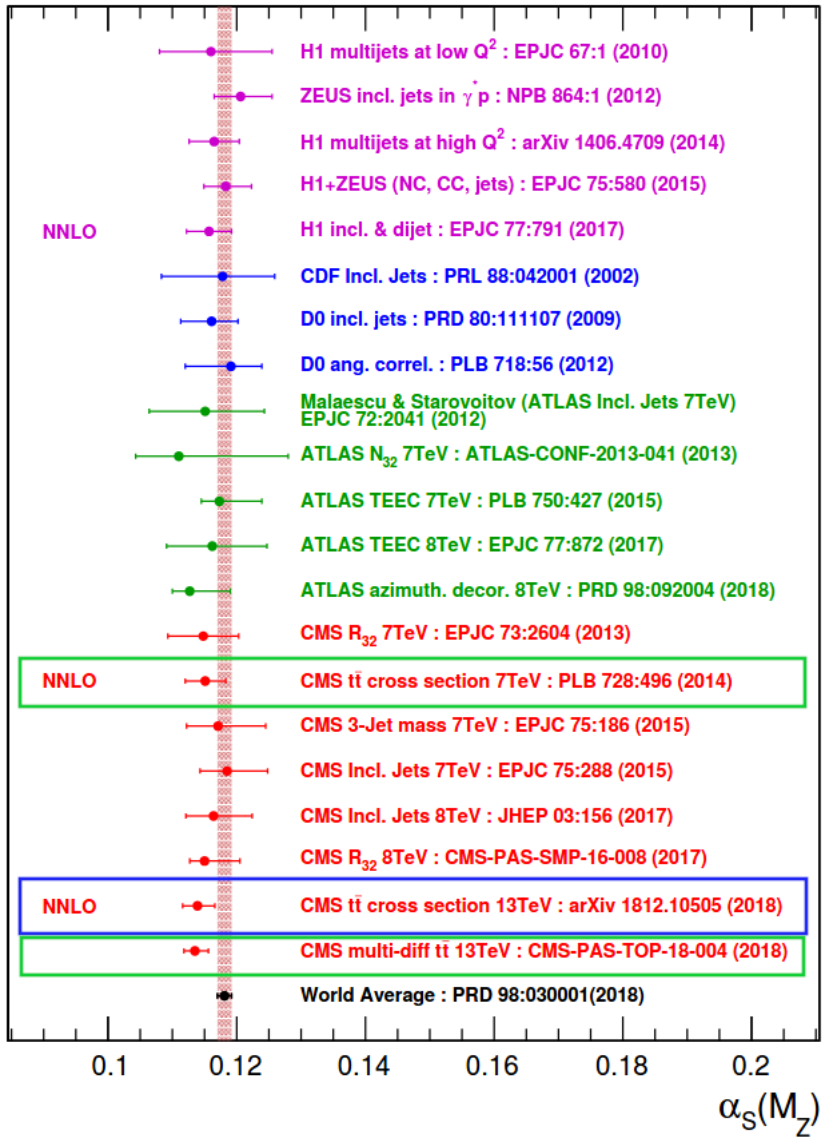

QCD parameters in PDF

	ABMP16	NNPDF3.1	CT14	MMHT14
m_t^{pole} [GeV]	170.37	172.5	173.3	174.2
RunDec loops	3	2	2	3
$m_t(m_t)$ [GeV]	160.86	162.56	163.30	163.47
$\alpha_S(m_Z)$	0.116	0.118	0.118	0.118
α_S range	0.112−0.120	0.108−0.124	0.111−0.123	0.108−0.128

- CT14 does not use $t\bar{t}$ data
- CT14 and MMHT14: uncertainties provided only for nominal PDF

PDF set	$\alpha_S(m_Z)$
ABMP16	0.1139 ± 0.0023 (fit + PDF) $^{+0.0014}_{-0.0001}$ (scale)
NNPDF3.1	0.1140 ± 0.0033 (fit + PDF) $^{+0.0021}_{-0.0002}$ (scale)
CT14	0.1148 ± 0.0032 (fit + PDF) $^{+0.0018}_{-0.0002}$ (scale)
MMHT14	0.1151 ± 0.0035 (fit + PDF) $^{+0.0020}_{-0.0002}$ (scale)

PDF set	$m_t(m_t)$ [GeV]
ABMP16	$161.6 \pm 1.6\,(\text{fit} + \text{PDF} + \alpha_S)\ ^{+0.1}_{-1.0}\,(\text{scale})$
NNPDF3.1	$164.5 \pm 1.6\,(\text{fit} + \text{PDF} + \alpha_S)\ ^{+0.1}_{-1.0}\,(\text{scale})$
CT14	$165.0 \pm 1.8\,(\text{fit} + \text{PDF} + \alpha_S)\ ^{+0.1}_{-1.0}\,(\text{scale})$
MMHT14	$164.9 \pm 1.8\,(\text{fit} + \text{PDF} + \alpha_S)\ ^{+0.1}_{-1.1}\,(\text{scale})$

PDF set	m_t^{pole} [GeV]
ABMP16	169.9 ± 1.8 (fit + PDF + α_S) $^{+0.8}_{-1.2}$ (scale)
NNPDF3.1	173.2 ± 1.9 (fit + PDF + α_S) $^{+0.9}_{-1.3}$ (scale)
CT14	173.7 ± 2.0 (fit + PDF + α_S) $^{+0.9}_{-1.4}$ (scale)
MMHT14	173.6 ± 1.9 (fit + PDF + α_S) $^{+0.9}_{-1.4}$ (scale)

parametrization - inclusive analysis

$\mathrm{t\bar{t}}$ topology exploited to derive precise parametrization of normalization and shape uncertainties

$$S_{1\mathrm{b}} = \mathcal{L} A_{\ell\ell} \sigma_{\mathrm{t\bar{t}}} \epsilon_{\ell\ell} 2\epsilon_{\mathrm{b}} (1 - C_{\mathrm{b}} \epsilon_{\mathrm{b}})$$
$$S_{2\mathrm{b}} = \mathcal{L} A_{\ell\ell} \sigma_{\mathrm{t\bar{t}}} \epsilon_{\ell\ell} \epsilon_{\mathrm{b}}^2 C_{\mathrm{b}}$$
$$S_{\mathrm{other}} = \mathcal{L} A_{\ell\ell} \sigma_{\mathrm{t\bar{t}}} \epsilon_{\ell\ell} \left[1 - 2\epsilon_{\mathrm{b}} (1 - C_{\mathrm{b}} \epsilon_{\mathrm{b}}) - \epsilon_{\mathrm{b}}^2 C_{\mathrm{b}}\right]$$

- $\epsilon_{\ell\ell}$ is the selection efficiency
- ϵ_{b} is the b-tagging efficiency
- C_{b} represents the residual correlation of tagging the two b-jets

- $A_{\ell\ell}$, $\epsilon_{\ell\ell}$, C_{b}, s_i, and b_i^j determined from simulation
- they depend on $\vec{\lambda}$
- b_i^j depends on ω_j

- S_{b}: normalization
- s_i / S_{b} shape

extrapol: $\frac{\Delta_i^{\pm}}{\sigma_{\mathrm{t\bar{t}}}} = \left| 1 - \frac{A^{\mathrm{fit}}}{A_i^{\pm}} \right|$

$$
\begin{aligned}
S^k_{1\mathrm{b}} &= \mathcal{L}\sigma^{(\mu_k)}_{\mathrm{t\bar{t}}} A^k_{\mathrm{sel}} \epsilon^k_{\mathrm{sel}} 2\epsilon^k_{\mathrm{b}}(1 - C^k_{\mathrm{b}}\epsilon^k_{\mathrm{b}}) \\
S^k_{2\mathrm{b}} &= \mathcal{L}\sigma^{(\mu_k)}_{\mathrm{t\bar{t}}} A^k_{\mathrm{sel}} \epsilon^k_{\mathrm{sel}} C^k_{\mathrm{b}}(\epsilon^k_{\mathrm{b}})^2 \\
S^k_{\mathrm{other}} &= \mathcal{L}\sigma^{(\mu_k)}_{\mathrm{t\bar{t}}} A^k_{\mathrm{sel}} \epsilon^k_{\mathrm{sel}} \left[1 - 2\epsilon^k_{\mathrm{b}}(1 - C^k_{\mathrm{b}}\epsilon^k_{\mathrm{b}}) - C^k_{\mathrm{b}}(\epsilon^k_{\mathrm{b}})^2\right]
\end{aligned}
$$

same as in inclusive analysis, but for each bin of $m_{\mathrm{t\bar{t}}}$ separately

$$L = \prod_i \frac{e^{-\nu_i} \nu_i^{n_i}}{n_i!} \prod_j \pi(\omega_j) \prod_m \pi(\lambda_m)$$

$$\nu_i = \sum_{k=1}^{4} s_i^k(\sigma_{t\bar{t}}^{(\mu_k)}, \vec{\lambda}, m_t^{MC}) + \sum_j b_i^j(\omega_j, \vec{\lambda})$$

ν_i incorporates the response matrix and its dependence on the nuisance parameters and m_t^{MC}

post-fit distributions of fit inputs - differential analysis

fit performed in categories of

1. b-tagged jet multiplicity
2. $m_{\mathrm{t\bar{t}}}^{\mathrm{reco}}$, including events with $N_{\mathrm{jets}} \leq 2$

- $m_{\ell\mathrm{b}}^{\mathrm{min}} \rightarrow m_{\mathrm{t}}^{\mathrm{MC}}$ and $m_{\mathrm{t}}^{\mathrm{kin}}$ (kin. reco)
- jet $\mathrm{p_T} \rightarrow$ JES

0 b-tags, no $m_{\mathrm{t\bar{t}}}^{\mathrm{reco}}$

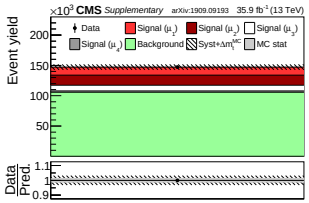

0 b-tags, $m_{\mathrm{t\bar{t}}}^{\mathrm{reco}}$ 1

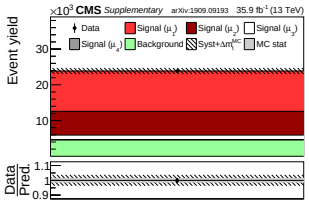

0 b-tags, $m_{\mathrm{t\bar{t}}}^{\mathrm{reco}}$ 2

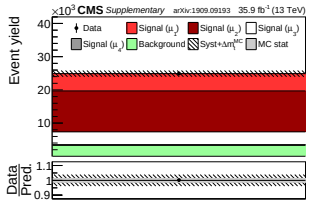

0 b-tags, $m_{\mathrm{t\bar{t}}}^{\mathrm{reco}}$ 3

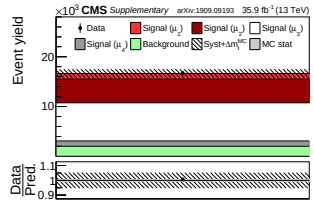

0 b-tags, $m_{\mathrm{t\bar{t}}}^{\mathrm{reco}}$ 4

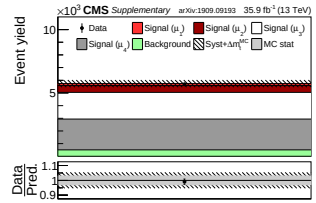

1 b-tag, no $m_{\mathrm{t\bar{t}}}^{\mathrm{reco}}$

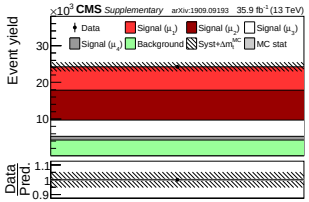

1 b-tag, $m_{\mathrm{t\bar{t}}}^{\mathrm{reco}}$ 1

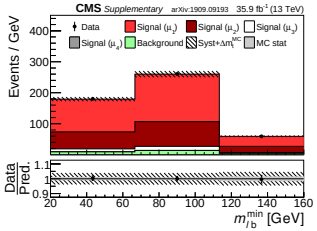

1 b-tag, $m_{\mathrm{t\bar{t}}}^{\mathrm{reco}}$ 2

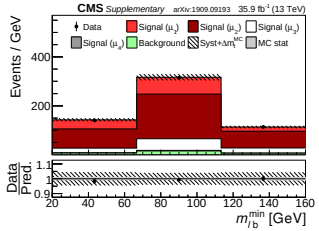

1 b-tag, $m_{\mathrm{t\bar{t}}}^{\mathrm{reco}}$ 3

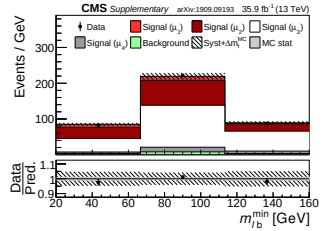

1 b-tag, $m_{\mathrm{t\bar{t}}}^{\mathrm{reco}}$ 4

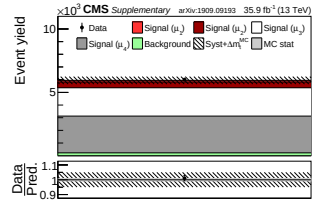

2 b-tags, $m_{\mathrm{t\bar{t}}}^{\mathrm{reco}}$ 1

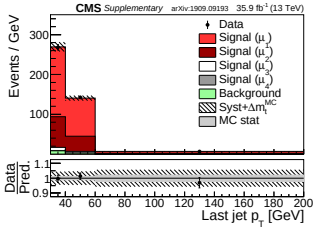

2 b-tags, $m_{\mathrm{t\bar{t}}}^{\mathrm{reco}}$ 2

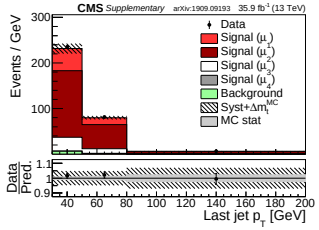

2 b-tags, $m_{\mathrm{t\bar{t}}}^{\mathrm{reco}}$ 3

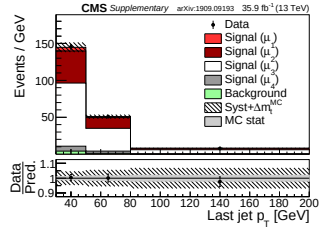

2 b-tags, $m_{\mathrm{t\bar{t}}}^{\mathrm{reco}}$ 4

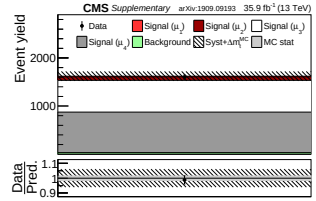

"no $m_{\mathrm{t\bar{t}}}^{\mathrm{reco}}$" = events with less than 2 jets

pulls and constraints - differential analysis (modelling)